



# Predicting grout's uniaxial compressive strength (UCS) for fully grouted rock bolting system by applying ensemble machine learning techniques

Shahab Hosseini<sup>1</sup> · Shima Entezam<sup>2,3</sup> · Behshad Jodeiri Shokri<sup>2,3</sup> · Ali Mirzaghobanali<sup>2,3</sup> · Hadi Nourizadeh<sup>2,3</sup> · Amin Motallebian<sup>2,3</sup> · Alireza Entezam<sup>2,3</sup> · Kevin McDougall<sup>4</sup> · Warna Karunasena<sup>2,3</sup> · Naj Aziz<sup>5</sup>

Received: 4 April 2023 / Accepted: 26 June 2024  
© The Author(s) 2024

## Abstract

This study proposes a novel system for accurately predicting grout's uniaxial compressive strength (UCS) in fully grouted rock bolting systems. To achieve this, a database comprising 73 UCS values with varying water-to-grout (W/G) ratios ranging from 22 to 42%, curing times from 1 to 28 days, the admixture of fly ash contents ranging from 0 to 30%, and two Australian commercial grouts, Stratabinder HS, and BU-100, was built after conducting comprehensive series of experimental tests. After building the dataset, a metaheuristic technique, the jellyfish search (JS) algorithm was employed to determine the weight of base models in the ensemble system. This system combined various data and modelling techniques to enhance the accuracy of the UCS predictions. What sets this technique apart is the comprehensive database and the innovative use of the JS algorithm to create a weighted averaging ensemble model, going beyond traditional methods for predicting grout strength. The proposed ensemble model was called the weighted averaging ensemble model (WAE-JS), in which the obtained results of several soft computing models such as multi-layer perceptron (MLP), Bayesian regularized (BR) neural networks, generalized feed-forward (GFF) neural networks, classification and regression tree (CART), and random forest (RF) were weighted based on JS and the new results were then generated. Eventually, the result of WAE-JS was compared to other models, including MLP, BR, GFF, CART, and RF, based on some statistical parameters, such as R-squared coefficients, RMSE, and VAF as indices for evaluating the performance and capability of the proposed model. The results suggested the superiority of the ensemble WAE-JS system over the base models. In addition, the proposed WAE-JS model effectively improved the predicting accuracy achieved from the MLP, BR, GFF, CART, and RF. Furthermore, the sensitivity analysis revealed that the W/G had the most significant impact on the grout's UCS values.

**Keyword** Uniaxial compressive strength · Grout · Rock bolting system · Machine learning methods

✉ Shima Entezam  
Shima.Entezam@unisq.edu.au

<sup>1</sup> Faculty of Engineering, Tarbiat Modares University, Tehran, Iran

<sup>2</sup> School of Engineering, University of Southern Queensland, Springfield Campus, Springfield, QLD 4300, Australia

<sup>3</sup> Centre for Future Materials (CFM), University of Southern Queensland, Toowoomba, QLD 4350, Australia

<sup>4</sup> School of Surveying and Built Environment, University of Southern Queensland, Toowoomba Campus, Toowoomba, QLD 4350, Australia

<sup>5</sup> School of Civil, Mining and Environmental Engineering, University of Wollongong, Wollongong, NSW 2500, Australia

## 1 Introduction

Fully grouted rock and cable bolting systems are the most common retaining systems widely employed in various civil and mining engineering aspects. Applications of rock bolting systems dates back to the late 1940s, which had been utilized as mining underground supports. However, the first use of cable bolts as a secondary support system in Australian underground coal mining was in the 1970s. Although rock bolting systems differ fundamentally and structurally from other types of reinforcement elements, demands utilizing these types of retaining systems are widespread and increased worldwide due to the simplicity,

availability of materials, and ease of installation process in the field [96, 97].

Although many parameters can affect the performance of the fully grouted rock and cable bolting systems, these retaining systems' success heavily depends on some influential parameters of grout, such as the quality, mechanical behaviours, and type of the grouts. In fact, grout acts as a stable interface between the retaining system, and surrounding rock mass with their loading transfer abilities [1]. In other words, grout plays a vital role as a medium to transfer the initiated stresses from bolt to stable rock mass and also to transfer the in situ stress (lateral confining stress) from surrounding rock to bolt-grout interface. Since the failure of the fully grouted rock bolting system occurs commonly at the bolt-grout interface [2]. As a result, some researchers focused on investigating the strength properties of grouts and their sample preparations for cable and rock bolting systems [1–15]. For instance, Aziz et al. [9] suggested a general standard for the preparation and testing procedures of various grouts and resins. Several crucial parameters, such as resin sample shape, size, height-to-width or diameter ratio (H/D), resin type, resin age, and curing time (CT), were investigated carefully. Also, some mechanical properties of resin, including the uniaxial compressive strength (UCS), elastic modulus (E), shear strength ( $\tau$ ), and creep, were examined. Li et al. [10] presented an analytical model for investigating a fully grouted cable bolt's shear behaviour, including shear strength and displacement. Mirza et al. [1] examined some mechanical parameters of two common grouts used in Australia, Jennmar Bottom-Up 100 (BU-100) and Orica Stratabinder HS. For this, the samples were cast on 50 mm cube moulds. The prepared samples were subsequently cured for 1 to 28 days. Then, the UCS, E, and rheological properties were measured. The results revealed that both grouts were suitable for applying in the cable bolting systems. Ma et al. [16] characterized the bond of fully grouted rock bolting systems based on the installation procedure. Mirzaghobanali et al. [17] investigated the mechanical behaviours of Stratabinder HS by casting and then curing small- and large-scale samples in cube and cylindrical moulds. The UCS values of cured samples, ranging from 1 to 28 days, were measured. Along with measuring UCS values, the bending resistance values of grouts were also determined by conducting four points bending test. In another research, Mirzaghobanali et al. [18] determined UCS values of grouts by considering a mixture of fly ash and Stratabinder HS, for different CTs. Indeed, this research was one of the early steps towards utilizing mine waste materials as a part of grout in the fully rock bolting systems. They found that the UCS and tensile strength of grouts had been increased in fly ash mixed samples. In another research, Entezam et al. [12] suggested

that the UCS values of grout and the axial bearing capacities of fully grouted rock bolting system resulting from pull-out tests, increased by replacing small amount of fly ash contents in the grout mixture.

Since the direct UCS experiments are extensively destructive, time- and cost-consuming, over the past two decades, several identified approaches, including empirical and statistical methods and intelligent machine learning techniques, have been proposed and developed as popular alternative methods for conventional direct UCS test, for predicting UCS values in different media. In addition to empirical techniques, numerous studies have explored the development of statistical models and formulas to estimate the UCS values (Table 1). However, addressing highly nonlinear issues, through purely statistical methods can be considered as a challenging task. As a result, the application of artificial intelligence (AI) and soft computing (SC) becomes effective and particularly relevant when addressing such a nonlinear relationship in different scopes of geosciences [19–33]. Some of the most significant research works to predict UCS values applying AI techniques in different medium were given as follows and in Table 2. For instance, Meulenkamp and Grima [34] applied artificial neural networks for predicting UCS values by considering physical properties such as hardness, porosity, density, and rock type information from hardness tests on rock samples. Sonmez et al. [35] predicted E and UCS values of Ankara Agglomerate by using regression and fuzzy logic methods. Tiryaki [36] applied regression and ANNs methods for predicting UCS and E values of the intact rock materials. Jahed Armaghani et al. [37] estimated UCS values by applying three AI techniques, including adaptive neuro-fuzzy inference system (ANFIS), ANNs, and nonlinear multiple regression (NLMR). A comparison of the results revealed that ANFIS was more reliable than the other methods. In another research, Jahed Armaghani et al. [38] presented a relationship for predicting the UCS of sandstone by considering some parameters, such as dry density, slake durability index, and Brazilian tensile strength. Moussas and Diamantis [39] predicted the UCS of serpentine by using ANNs. For this, they considered serpentinization percentage and physical, dynamic, and mechanical characteristics of serpentinites as input data, while UCS values were the outputs. In another research, Moussas and Diamantis [40] applied ANN technique to estimate UCS values of peridotites. Cao et al. [41] presented a new hybrid AI method called the XGBoost-FA model, which was a combined model of the extreme gradient boosting machine (XGBoost) with the firefly algorithm (FA). The method was employed for predicting UCS and E values. Gowida et al. [42] utilized three AI methods, including ANNs, ANFIS, and support vector machine (SVM), to estimate UCS's downhole formation by

**Table 1** Various techniques for UCS prediction

Year	Author(s)	Method(s)	References
2014	Azimian et al.	MR	[43]
2015	Mohamad et al.	Empirical, NLMR, ANN, ANFIS	[44]
2015	Najibi et al.	Empirical	[45]
2015	Tandon et al.	Empirical	[46]
2015	Ng et al.	MR	[47]
2016	Fereidooni et al.	Empirical	[48]
2017	Jalali et al.	MR, ANFIS	[49]
2017	Sharma et al.	MR	[50]
2018	Heidari et al.	Empirical, MR, FIS	[51]
2018	Aboutaleb et al.	MR, ANN, SVR	[52]
2018	Ghasemi et al.	Model tree (MSP Algorithm)	[53]
2019	Saeidi et al.	FIS	[54]
2019	Aliyu et al.	Empirical	[55]
2020	Teymen and Mengüç	GEP, ANN, ANFIS	[56]
2021	Mahmoodzadeh et al.	DNN, DT, SVR	[57]
2023	Xu et al.	SSA-XGBoost	[58]
2023	Liu et al.	MR, RF, DT	[59]

*MR* multiple regression, *FIS* fuzzy inference system, *GEP* gene expression programming, *ANN* artificial neural network, *ANFIS* adaptive neuro-fuzzy inference system, *DNN* deep neural network, *DT* decision tree, *SVR* support vector regression, *RF* random forest

**Table 2** Range of effective parameters

Parameters	Symbol	Unit	Minimum	Mean	Maximum	SD
Curing time	<i>CT</i>	day	1	13.463	28	8.884
Water-to-grout ratio	<i>W/G</i>	%	22	34.463	42	3.452
Stratabinder HS	<i>GS</i>	%	0	75.833	100	33.488
BU-100	<i>GBU</i>	%	0	9.259	100	29.258
Fly ash content	<i>GF</i>	%	0	9.352	30	10.861
UCS	<i>UCS</i>	MPa	22.58	60.381	90.32	17.602

considering drilling mechanical properties such as rate of penetration (ROP), gallon per minute (GPM), standpipe pressure (SPP), rotating speed in revolution per minute (RPM), torque (T), and weight on bit (WOB).

As mentioned, the AI and SC techniques are being applied to predict the UCS values. It is noteworthy that some of these AI optimization techniques, such as ANN, FIS, are available as the first options where complicated simulations are needed. However, training and testing procedures might be intensively time-consuming process. Moreover, the predictions would be more accurate than the other methods with lower errors if ensemble models were selected. This is because of combining outputs resulting from multiple techniques. Due to the importance of exact UCS values, this research introduced novel ensemble modelling approach for predicting the UCS values of grout in fully grouted rock bolting systems. Along with applying ensemble modelling, jellyfish search (JS) algorithm, which is innovative and distinguish, has been used to create

weighted averaging ensemble predictions. Indeed, the results from other SC techniques, including multi-layer perceptron (MLP), Bayesian regularized (BR) neural networks, generalized feed-forward (GFF) neural networks, classification and regression tree (CART), and RF, will be combined to achieve more reliable and robust predictive system.

The literature reviews and Table 2 revealed that although many researchers applied soft computing techniques for predicting the UCS values of rocks, these methods have yet to be used for estimating the UCS values of grouts in bolt or cable systems. It is because of the difference in the material, complex composition, and mechanical behaviour. For instance, in comparison with the rocks that come with monolithic minerals, some of the other components, such as fly ash, cement, or water, might be found in the grout. Moreover, SC models suitable for the rocks might not consider the time-dependent behaviour of grout or the influence of environmental factors like

temperature and humidity. The lack of comprehensive datasets is one of the other main reasons that should be mentioned. Indeed, building a robust soft computing model requires a substantial amount of data for training and validation. While datasets might be available for predicting the UCS of rocks, similar datasets for grouts in bolt or cable systems may need to be expanded or more present. As a result, as mentioned in the paper, one of the aims of this research is to build a dataset and showcase the performance of SC methods as a reliable tool instead of applying time- and cost-consuming conventional laboratory tests in predicting UCS values of grout in rock and cable bolting system, a valuable contribution to both academia and industry. Therefore, the main objective of this paper is (a) to build a dataset by considering CTs, water-to-grout (W/G) ratios, and the type of cementitious grouts (2) to predict the exact UCS values of grouts used in either rock or cable systems with suggesting ensemble methods.

## 2 Experimental analysis

### 2.1 UCS tests

Seventy-three tests have been conducted to investigate the UCS values of different grouts for fully grouted rock bolting systems. For this, two common Australian grouts, including Stratabinder HS and BU-100, were chosen for further investigations. Six different amount of fly ash contents, including 5%, 10%, 15%, 20%, 25%, and 30%, were used in the grouts to investigate the effect of them on mechanical behaviour of grouts specifically UCS values. Also, to cover common various mixtures of grouts, eight different W/G ratios of grouts including, 22%, 25%, 30%, 32%, 35%, 36%, 38%, and 40%, have been considered in the required tests. The grout samples were then prepared and cast into the cube moulds with 50 mm × 50 mm × 50 mm dimensions in a line with ASTM standard C579 [60]. Subsequently, the samples were cured at five different times, 1, 7, 14, 21, and 28 days. Grout preparation and a view of moulds in one of the conducted tests are shown in Fig. 1.

After the curing procedure, the UCS values have been measured by a compression testing machine made by an impact test equipment, under a displacement of 1 (mm/min) at the University of Southern Queensland. Figure 2 shows a sample before and after the test.

## 3 Material and methods

### 3.1 Classification and regression tree (CART)

Classification and regression tree (CART) is one of the decision tree algorithms categorized in the data mining techniques by Li et al. [61]. This technique belongs to the rules-based technique that can provide binary trees for recursively dividing a prediction space into subsets. Unlike other machine learning methods, the CART is a “white box” procedure that simplifies the relationships between the inputs and output(s) [62]. Instead of considering the relationships between the variables, the CART algorithm dataset is divided into uniform parts based on yes/no responses concerning the predictor values with the CART algorithm. This process leads to the creation of a binary tree. If the dependent variable is quantitative, the structured tree will be representative of a regression tree. However, if it is qualitative, it is representative of a classification tree. In the recursive partition process, at the starting point exists a root node, which includes the whole dataset and represents an attribute or input variable. Whereas branches surround the sides of each root, each shows a range of values. Figure 3 shows a general structure of a simple CART tree. The nodes are comprised of a till and leaf that predicts model output at the end of each step. This structure will continue till the termination criteria are met. It is worth noting that defining the optimum value for the number of intervals and the maximum tree depth will control the overgrowth of produced trees and overfitting problems.

### 3.2 RF

RF algorithm, which is generally recognized as a robust nonparametric statistical technique for classification and regression issues, was first proposed by Breiman [63]. Compared to other SC techniques, RF was developed as an ensemble approach relying on the outcomes from several trees to obtain prediction accuracy. Indeed, the RF integrates the estimated values from structured trees in the forests to provide the optimal result for each generated observation. Each tree in the forest serves as a vote for the RF's ultimate decision [63]. Figure 4 illustrates the general scheme of the RF algorithm.

### 3.3 ANN

In 1949, ANN was first constructed using the biological neural network as its primary source of inspiration. ANNs



Fig. 1 a Grout preparation and b a view of UCS samples in the curing room



Fig. 2 A sample before and after the UCS test

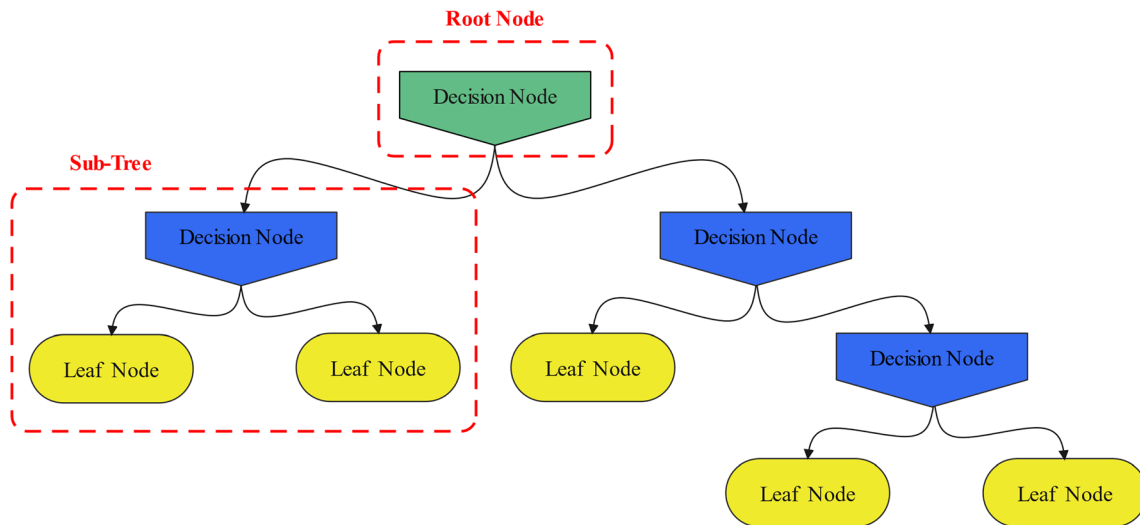


Fig. 3 Structure of simple CART tree

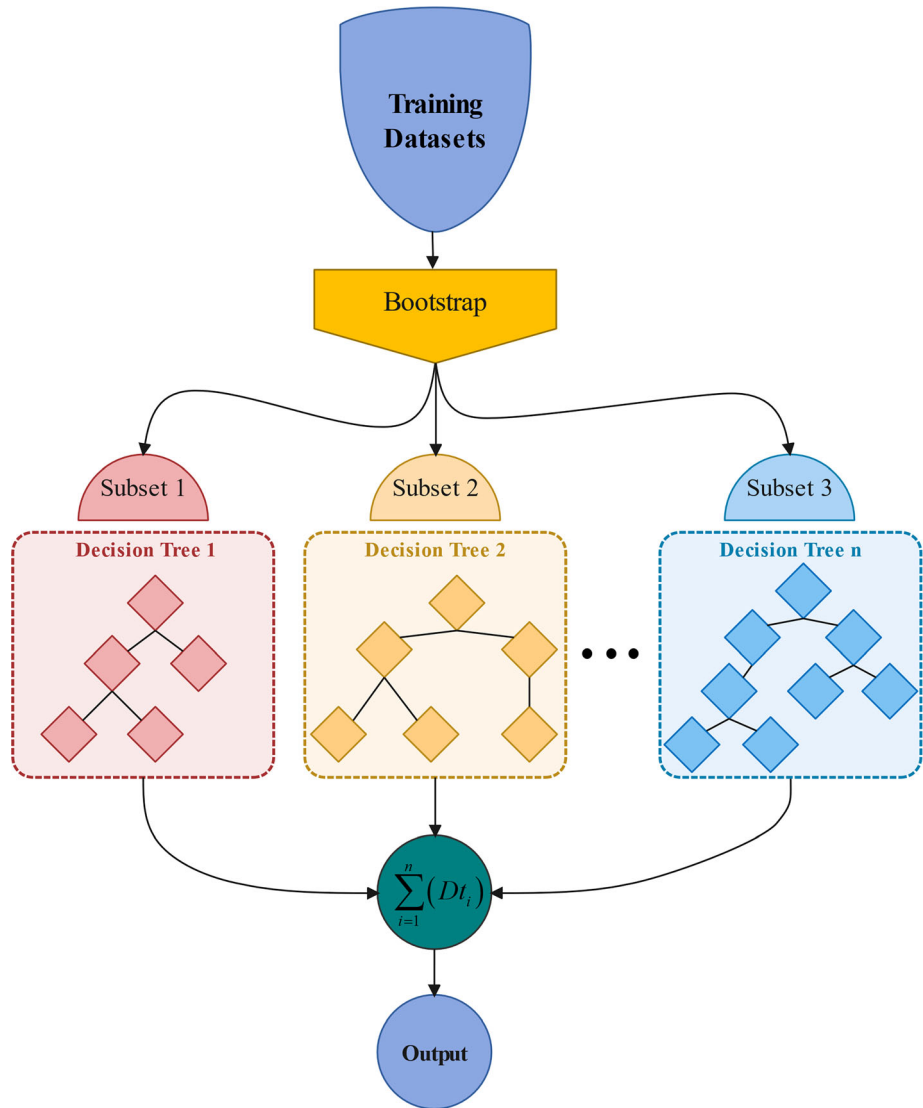
are noticeably superior, which may be attributed to the fact that nonlinear mapping can be carried out across a dataset when utilizing it. The ANN splits the available data into three primary datasets: training, testing, and validating data. The performance of ANN is controlled by three following factors, including transfer functions, the number of epochs, and learning roles. The ANN generally consists of

three main layers, including the input, the output, and the hidden layers [64].

### 3.3.1 Multi-layer perceptron (MLP)

The MLP is one of the most widely used ANNs that are being applied in different scopes. The MLP neural network

**Fig. 4** General scheme of the RF algorithm



should first be trained to predict targets, which this process is commonly performed by utilizing the feed-forward back-propagation (FFBP) learning algorithm [65]. This algorithm minimizes the system errors between the predicted and actual values. In the MLP, a more compatible output may be generated by the system’s parameters of after its iterations have been mastered. The number of hidden layers is generally determined based on a trial and error and also depends on the complexity of the problem [66]. The general scheme of MLP structure is shown in Fig. 5. The output values of the MLP will be determined using the following equation [67]:

$$y = f_i \left( \sum_{j=1}^n w_{ij}x_j + b_i \right) \tag{1}$$

In which,  $x$  and  $y$  are, respectively, the value of inputs and output(s),  $w$  stands the weight vector,  $b$  shows the bias

connected to the layers, and  $f$  denotes the transfer function (tansig, logsig, purelin, radbas, etc.).

### 3.3.2 Bayesian regularized (BR) neural network

The Bayesian regularized algorithm was first introduced by MacKay in 1992 as a solution to problems like determining the optimum hidden neurons while constructing ANN topology. He applied Bayes’ theorem to the regularization process [68]. The BR neural network is a variety of propagation neural networks that combine the traditional sum of the least-squares error function (Fig. 6) [69]:

$$E_D = \sum_{i=1}^n (y_i - t_i)^2 = \sum_{i=1}^n (e_i)^2 \tag{2}$$

$$S(w) = \beta E_D + \alpha E_W \tag{3}$$

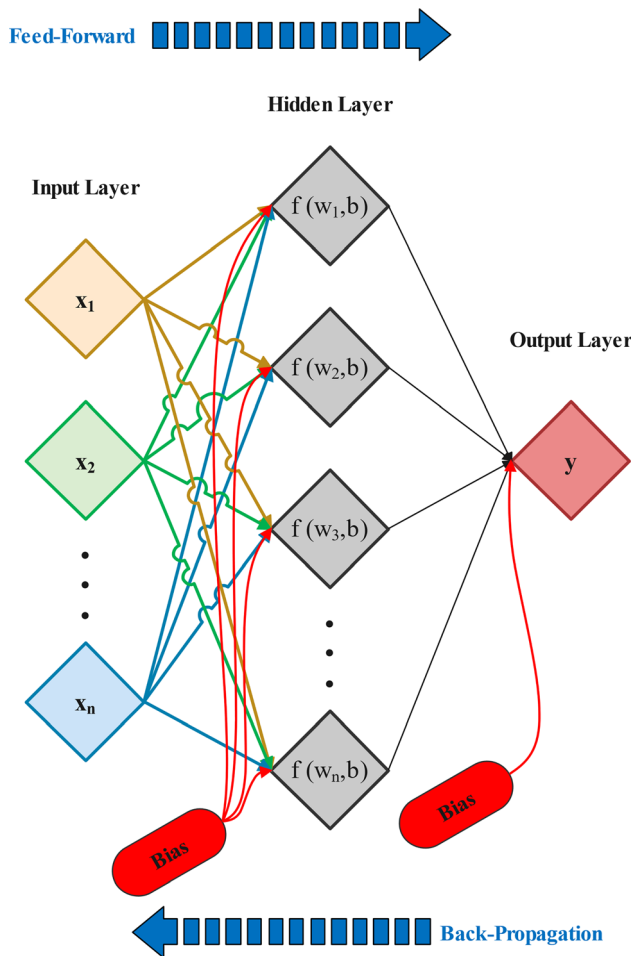


Fig. 5 General architecture of the MLP model

$$E_w = \sum_{i=1}^m w_i^2 \tag{4}$$

whereas  $n$  and  $t$  denote the number of training data and the target values, respectively,  $\alpha$  and  $\beta$  are hyperparameters (regularization parameters),  $E_w$  suggests penalty phrase (large penalizer values of the weights),  $m$  indicates the number of weights, and  $S(w)$  signifies the performance function of the network [70].

### 3.3.3 Generalized feed-forward (GFF) neural networks

GFF neural networks are generalizations of MLPNNs that allow for connecting one or more layers. Although the GFF neural network works theoretically similarly to MLPNN, it eliminates the complexity of the systems rather than MLPNN does. Besides that, MLPNN has often been trained hundreds of times, adding more learning epochs to externally elucidate the problem. However, GAFFNN uses only a few numbers of training epochs (Fig. 7) [71].

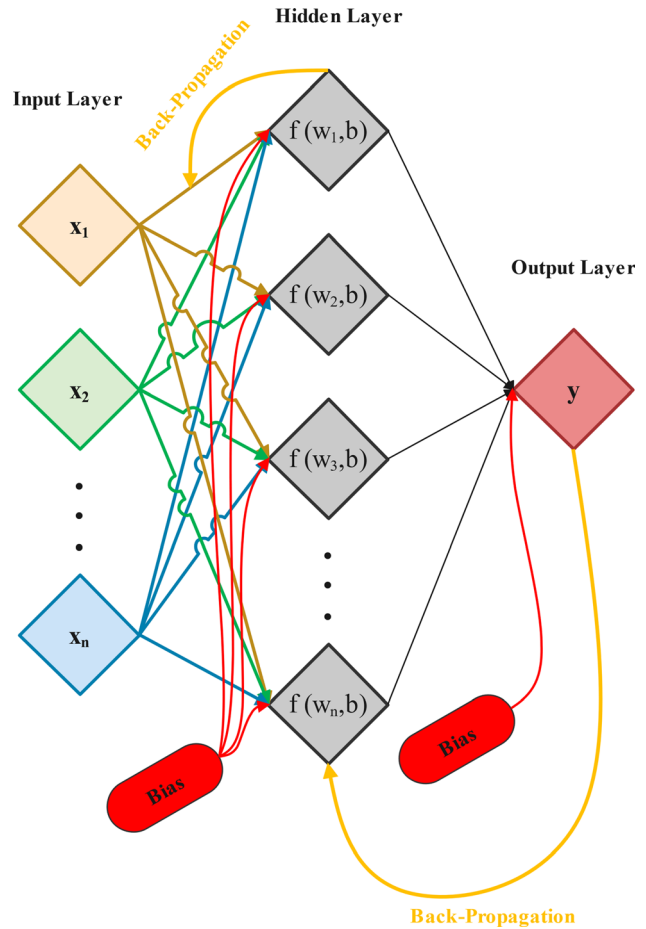


Fig. 6 Topology of the BR neural network model

## 3.4 Ensemble model

As mentioned before, ensemble machine learning (EML) techniques have been used for predicting UCS values in this article. Indeed, the EML model integrates several base models called sub-models. The integration process includes four following methods: simple averaging, weighted averaging, integrated stacking, and separate stacking ensemble models. Also, bagging and boosting methods can be applied for implementing super learner ensembles.

### 3.4.1 Sub-models

Sub-models can be provided by employing one of the AI methods. Indeed, the average of these basic models, which have different structures, is required. For instance, an ANN model has  $n$  basic MLP, which has different hidden layers, transfer functions, and optimizers.

**3.4.1.1 Weighted averaging ensemble** Due to the equal weights allocated for each sub-model, the predicted values were improved in the SAE technique. Moreover, the

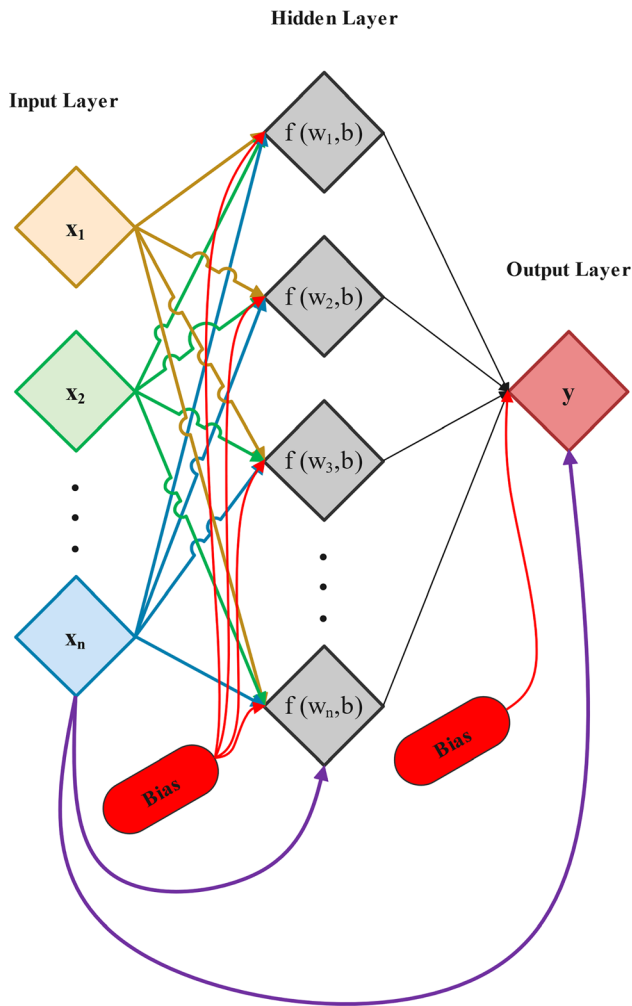


Fig. 7 Structure of GFF neural network

weighted averaging ensemble (WAE) combined results by averaging the outputs for all basic models (Fig. 8). It is noteworthy that the weight of the sub-model is determined by applying optimizing algorithms.

#### 4 Jellyfish search (JS) algorithm

In general, metaheuristics algorithms can be divided in two categories, including nature inspired and human inspired. The nature-inspired metaheuristic algorithms can be categorized in three sub-classes as evolutionary, physical-based, and swarm-based algorithms [72]. In this research, JSO was chosen instead of applying other evolutionary algorithms such as genetic algorithms (GA) [73], physical-based algorithm such as gravitational search algorithm (GSA) [74], or swarm-based algorithm such as particle swarm optimization (PSO) [75]. It is because of its unique

biological inspiration, diversity, adaptability, scalability, convergence speed, parallelism, and ability to strike an effective balance between exploration and exploitation [67]. In 2020, the jellyfish search (JS) algorithm was firstly proposed by Chou and Truong [72] by identifying and monitoring jellyfish food-searching behaviour in oceans. Since the proposal of the jellyfish search (JS) algorithm, several research works have applied it in diverse fields [76–83]. For instance, Abdel-Basset et al. [76] applied JS algorithm to optimize photovoltaic (PV) system in solar/PV generating units. Gouda et al. [78] could solve the identifications problems of polymer exchange membrane fuel cells (PEMFCs) model. Durmus et al. [84] applied the JS with other swarm-based algorithms, such as PSO, artificial bee colony (ABC), and mayfly algorithm (MA), to determine the optimal design of linear antenna arrays in wireless communication. Throung and Chou [79] presented a new model of fuzzy adaptive jellyfish search-optimized stacking system (FAJS-SS) for solving and optimizing engineering planning and designs. Ansari et al. [82] used JS algorithm to estimate state of health (SOH) of lithium-ion batteries. JS algorithm was proposed by identifying and monitoring jellyfish food-searching behaviour in oceans. Jellyfish foods include phytoplankton, small fish, and fish eggs, which are small oceanic animals [85]. Jellyfish bloom refers to a large mass of jellyfish that can swarm [86]. The ocean current and each jellyfish's personal search inside the jellyfish bloom are the two primary searching mechanisms of jellyfish for food that govern how the jellyfish's mechanism for looking for food moves. A giant jellyfish bloom might develop under these circumstances due to abundant nutrients in the ocean [87]. Each jellyfish is around its current area simultaneously to locate a spot with more food. The global and local search capabilities of the JS algorithm are shown by the mobility of jellyfish based on ocean currents and the search of each jellyfish in the jellyfish bloom, respectively. An ocean current often starts a jellyfish bloom, but if the environment changes (for instance, due to wind or temperature), the jellyfish travel to another ocean current [67]. The JS algorithm follows six primary phases: (1) jellyfish in the ocean, (2) ocean current, (3) jellyfish swarm, (4) passive motions, (4) active motions, and (6) jellyfish bloom [88]. Equation 5 is used in the JS method to determine the ocean current [72].

$$\overrightarrow{\text{trend}} = X^* - (\beta \times \text{rand} \times \overline{X}) \quad (5)$$

In which  $X^*$  denotes the position of the jellyfish with a maximum food source representing the best solution,  $\beta$  stands as a distributions factor,  $\text{rand}$  signifies values in the range [0, 1] that are randomly determined, and  $\overline{X}$  indicates



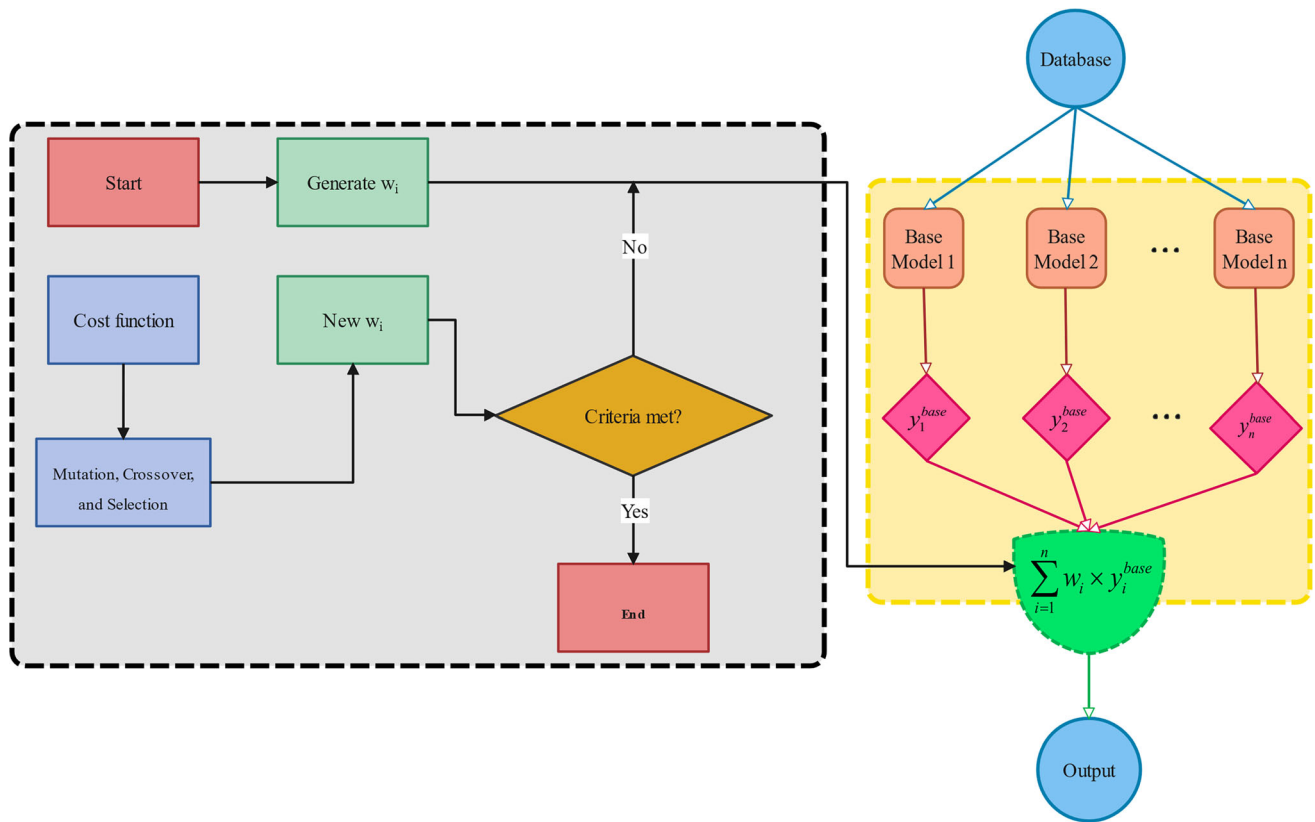


Fig. 8 Diagram of the WAE-DE hybrid algorithm

the mean food source in the jellyfish bloom. Eventually, each jellyfish’s location was given by Eq. 6 [72].

$$X_i^{t+1} = X_i^t + (\text{rand} \times \overrightarrow{\text{trend}}) \tag{6}$$

In other words, Eq. 6 determines how the JS algorithm’s exploration step (global searches) operates. The jellyfish bloom’s local search step is carried out by two different kinds of motion: passive and active motion. The passive motion involves each JS rotating around its location, comparing the amount of food in the new locations to its current location, and moving towards the new location if there is much more food available. Each jellyfish ( $X_i$ ) in the active movement compares its location to another one ( $X_j$ ), and if the amount of food at  $X_j$  is greater than that at  $X_i$ , the jellyfish moves towards  $X_j$ . Otherwise, it will veer away from the  $X_j$  jellyfish. JS algorithm uses Eq. 30 to perform the passive movement [89].

$$X_i^{t+1} = X_i^t + (\gamma \times \text{rand} \times (U^b - L^b)) \tag{7}$$

where  $U^b$  and  $L^b$  denote the upper and lower bounds of the search space, respectively, and  $\gamma$  is the motion parameter.

To accomplish its active motion, each jellyfish uses Eq. 8 [72].

$$X_i^{t+1} = \begin{cases} \text{if } F_f(X_j) \leq F_f(X_i^t) & X_i^t + (\text{rand} \times (X_j - X_i^t)) \\ \text{if } F_f(X_j) > F_f(X_i^t) & X_i^t + (\text{rand} \times (X_i^t - X_j)) \end{cases} \tag{8}$$

In which  $F_f$  is the fitness function. Equation 9 suggests a time management process for the JS algorithm to balance the exploration and exploitation mechanism. The random value  $c(t)$  fluctuates between 0 and 1 [72].

$$c(t) = \left| \left( 1 - \frac{t}{\text{Max}_{\text{iteration}}} \right) \times (2 \times \text{rand} - 1) \right| \tag{9}$$

where the current iteration number,  $t$ , is indicated in Eq. 9. When the values of  $c(t)$  exceed 0.5, the jellyfish conduct the global searches; otherwise, they conduct the local searches. The function  $(1-c(t))$  regulates the jellyfish’s passive and active motions. When the value of  $\text{rand}$  exceeds  $1-c(t)$ , the jellyfish move passively; otherwise, they move in active situations. According to Eq. 9,  $c(t)$  and  $1 - c(t)$  tend to be one and zero as time passes, respectively. This means that the JS algorithm’s capability to be exploited increases over time. The chaotic logistic map generates the initial population for the JS algorithm at random. The logistic map method (Eq. 10) makes it

possible to produce an initial population with a wide variety of models, which aids in the algorithm’s quick convergence rate [72].

$$X^{i+1} = rX^i(1 - X^i), \begin{cases} 0 \leq X^0 \leq 1, r = 4.0 \\ X^0 \notin (0.0, 0.25, 0.50, 0.75, 1.0) \end{cases} \quad (10)$$

## 5 Data analysis and data preparation

### 5.1 Data presentation

Statistical analysis is needed to show the data and interpretation graphically. For this, five influential parameters were chosen as independent variables for estimating the UCS values of the grout in the fully grouted rock bolting system. The dataset includes seventy-three measurements of CT, W/G, Stratabinder HS (GS), BU-100 (GBU), fly ash (GF) contents, and UCS values. Table 2 provides descriptive statistics of the inputs and output parameters. The CT values range between 1 and 28 days with different values of W/G ratios, ranging from 22 to 42%. Notably, the GS, GB, and GF values were 0–100%, 0–100%, and 0–30%, respectively. Moreover, the measured UCS values ranges were between 22.58 and 90.32 MPa.

The Pearson correlation between effective parameters is depicted in Fig. 9. As can be seen, the correlation between UCS and CT is 0.71, which represents a high positive relation. Whereas a value of  $-0.0089$  is calculated for the correlation between UCS and GS, where indicating a low negative relation. Figure 10 shows the matrix plot of effective parameters.

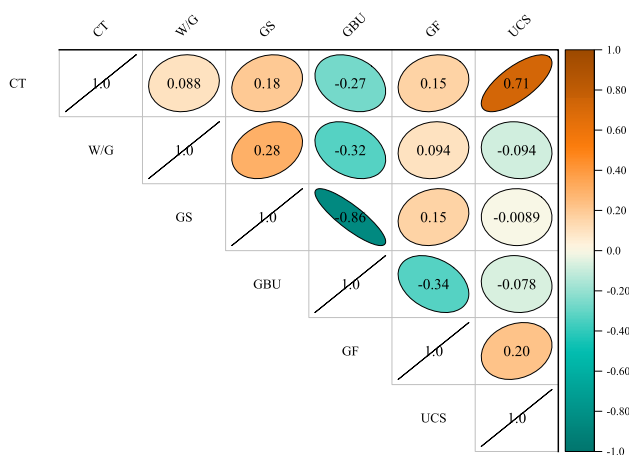


Fig. 9 Pearson correlation between effective parameters

## 6 Results and discussions

This study addresses the performance and accuracy of several powerful machine learning (ML) techniques, including MLP, BR, GFF, CART, and RF, methods to predict UCS values of grout in the fully grouted rock bolting system. For this, the measured data were standardized and normalized to allow the model’s generating. For this, available data were normalized by the min–max normalized method, which reduces data ranges to 0 to 1 value (Eq. 11) [90]:

$$X_n = \frac{X_m - X_{\min}}{X_{\max} - X_{\min}} \quad (11)$$

In which  $x_n$  stands the normalized value of  $x$ ,  $x_{\max}$  represents the maximum value of data,  $x_{\min}$  is the minimum value of data, and  $x_m$  signifies the actual values of the data.

After normalizing the data, the training and testing datasets were subsequently built based on random selections. The training dataset included 54 data (or 75% of the dataset), whereas the testing dataset consisted of 25% of the dataset (or 18 data). The ANN, CART, and RF models were created using the datasets supplied in the normalization stage. As a result, the model parameters are changed at the point of prediction to achieve the maximum accuracy and performance of the models. The ideal structures of employed AI techniques were found after comparing the results with applying the following statistical criteria, including determination coefficient (R-squared), value account for (VAF), and root mean square of errors (RMSE) (Eqs. 12–14) [71, 90–94].

$$R^2 = 1 - \left( \frac{\sum_{i=1}^n (O_i - P_i)^2}{\sum_{i=1}^n (P_i - \bar{P}_i)^2} \right) \quad (12)$$

$$RMSE = \sqrt{\frac{1}{n} \sum_{i=1}^n (O_i - P_i)^2} \quad (13)$$

$$VAF = 100 \cdot \left( 1 - \frac{\text{var}(O_i - P_i)}{\text{var}(O_i)} \right) \quad (14)$$

where  $O_i$  and  $P_i$  are measured and predicted values, respectively.  $\bar{P}_i$  is mean value of the estimated value.  $n$  represents the number of available data.

The next step was to compare and evaluate the level of performance of various developed models using the final rating of the model (FRM) and colour intensity system (CIS). The  $R^2$ , RMSE, and VAF values were rated during the FRM procedure. The model with the highest  $R^2$  and VAF values and the lowest RMSE value was deemed to have the highest rate. It is noteworthy that the highest rate depends on the number of models obtained. For instance, if there are ten models, the top model will have a rating of 10

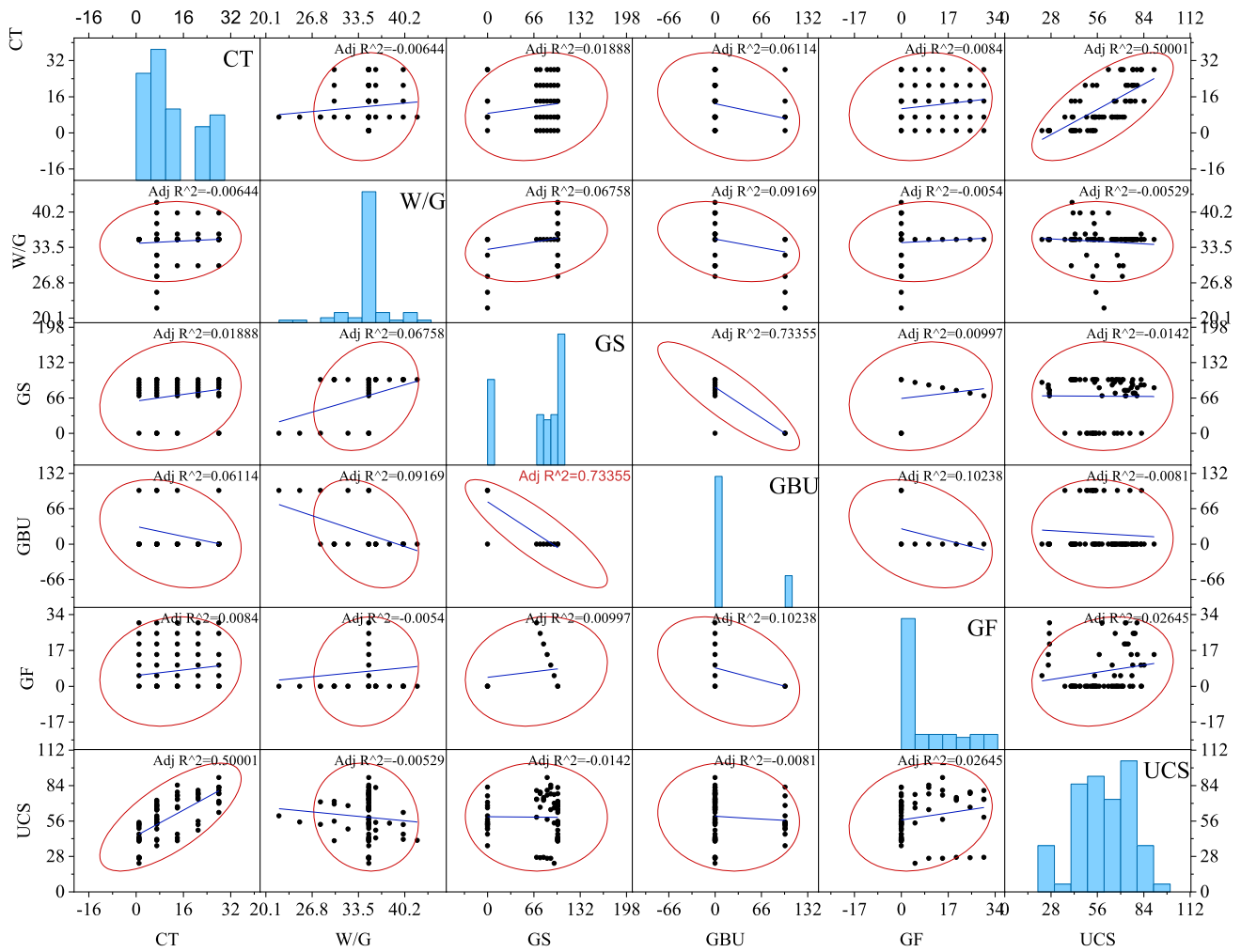


Fig. 10 Matrix plot of effective parameters

[95]. Equation (15) is used for formulating the FRM rating system.

$$FRM = \sum_{i=1}^2 (r_i^{R^2} + r_i^{RMSE} + r_i^{VAF}) \quad (15)$$

where  $r_i$  is the rate of statistical indices,  $i$  means 1 for training rates of statistical indices or 2 for testing rates of statistical indices.

### 6.1 Developing CART model

To develop CART model, the XLSTAT software was employed for predicting UCS values. In order to attain a high-accuracy level and minimal errors, the CART algorithm uses of train datasets to attempt to understand the connection between the inputs and output(s). Also, the model’s performance is evaluated using the testing dataset. In this study, two stopping criteria, i.e. the maximum tree depth and the number of intervals, were considered after

introducing datasets to the software to prevent the model’s complexity.

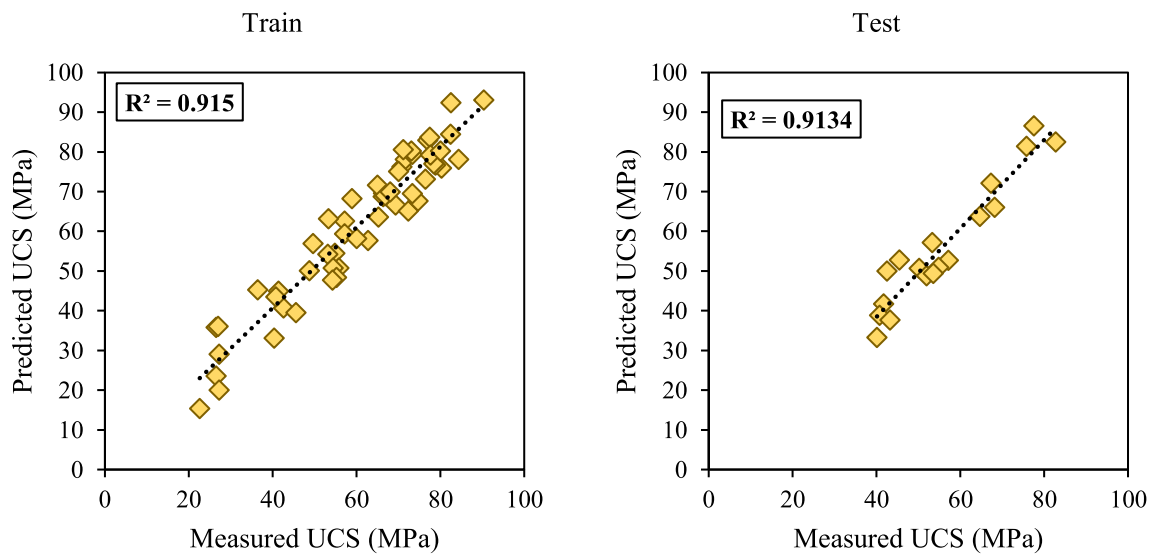
Since choosing the large values causes overfitting and excessive tree growth, the general range of 1–10 for both maximum tree depth and the number of intervals was selected. Through trial and error, the initial ranges for the maximum tree depth and the number of intervals were lowered to (4–8) and (3–8) to achieve the best possible combination of these two parameters. Subsequently,  $R^2$ , RMSE, and VAF values related to each model were calculated for the training and testing datasets (Table 3). Following this, seven models were then examined, each with a different value for the stopping criteria. Afterwards, the simple ranking of the FRM technique was used to select the most accurate model. The results of structured CART models with the various maximum tree depth and the number of intervals. The specified scores for them are presented in Table 3. As found in Table 3, the best CART model with high performance is model number 5, shown in bold, with a total rate of 42 of 42. The correlation between

**Table 3** Obtained performance indices and their rates for CART models

Model	No	Maximum tree depth	Number of intervals	Performance indices					
				Train			Test		
				$R^2$	RMSE	VAF	$R^2$	RMSE	VAF
CART	1	4	3	0.882	4.836	90.334	0.836	2.457	86.819
	2	4	4	0.882	4.880	90.323	0.802	2.425	86.875
	3	5	5	0.871	4.869	90.278	0.825	2.435	86.842
	4	6	6	0.907	4.858	90.278	0.836	2.426	86.875
	<b>5</b>	<b>7</b>	<b>7</b>	<b>0.915</b>	<b>4.835</b>	<b>90.389</b>	<b>0.913</b>	<b>2.424</b>	<b>86.930</b>
	6	8	8	0.912	4.869	90.300	0.847	2.426	86.842
	7	8	9	0.871	4.880	90.278	0.813	2.428	86.842

No	Maximum tree depth	Number of intervals	Rating for performance indices						Total rate
			Train			Test			
			Rating for $R^2$	Rating for RMSE	Rating for VAF	Rating for $R^2$	Rating for RMSE	Rating for VAF	
1	4	3	3	6	6	4	1	1	21
2	4	4	3	1	5	1	6	5	21
3	5	5	1	3	1	3	2	2	12
4	6	6	5	5	1	4	4	5	24
<b>5</b>	<b>7</b>	<b>7</b>	<b>7</b>	<b>7</b>	<b>7</b>	<b>7</b>	<b>7</b>	<b>7</b>	<b>42</b>
6	8	8	6	3	4	6	5	2	26
7	8	9	1	1	1	2	3	2	10



**Fig. 11** Measured UCS values compared to predicted one by the CART model

measured and predicted UCS values using the CART model for training and testing parts is shown in Fig. 11.

### 6.2 Developing RF model

The RF models with the different  $n_{tree}$  and  $m_{try}$  values as two main stopping criteria were obtained. These stopping criteria control the system’s complexity and reduce the model’s running time. Therefore, the range of 50 to 200 was considered for  $n_{tree}$ , and  $m_{try}$  was selected as 4, 6, and 8. The RF models were developed applying these settings (Table 4). According to Table 4, the 12 various RF models were constructed for predicting the UCS values, whereas only one was suitable for high-accuracy UCS prediction. Therefore, like the CART process, the Zorlu technique and FRM rating system were used to select a model with the

highest score. Model no. 3 was one of the RF models that provided better RMSE than other RF models. However, the rating system and total rate indicated that RF model no. 9 was the superior model to estimate UCS values, with a total rate of 69 out of 72 (Table 4). Hence, it can be concluded that RF model no. 9 with  $n_{tree} = 200$  and  $m_{try} = 8$  was the most accurate model, shown in the Table 4. The measured and predicted UCS values by RF method in the training and testing phases are depicted in Fig. 12. This figure showed that the RF model’s performance was more than that of the CART model. Therefore, the RF model predicts the UCS values better than the CART model.

**Table 4** Obtained performance indices and their rates for RF models

Model	No	$n_{tree}$	$m_{try}$	Performance indices					
				Train			Test		
				$R^2$	RMSE	VAF	$R^2$	RMSE	VAF
RF	1	200	4	0.845	4.972	91.029	0.768	2.839	84.018
	2	150	4	0.792	4.932	91.015	0.768	2.739	84.018
	3	100	4	0.805	4.732	91.029	0.741	2.906	83.978
	4	50	4	0.805	4.972	91.029	0.741	2.839	83.978
	5	200	6	0.819	4.972	91.002	0.741	2.792	84.018
	6	150	6	0.859	4.865	91.069	0.808	2.892	83.964
	7	100	6	0.832	4.958	91.055	0.781	2.906	84.004
	8	50	6	0.845	4.985	91.029	0.768	2.879	83.991
	<b>9</b>	<b>200</b>	<b>8</b>	<b>0.9254</b>	<b>4.8516</b>	<b>91.14</b>	<b>0.875</b>	<b>2.772</b>	<b>84.098</b>
	10	150	8	0.859	4.932	91.015	0.768	2.866	83.978
	11	100	8	0.819	4.958	91.055	0.795	2.706	84.018
	12	50	8	0.792	4.985	91.042	0.781	2.879	83.991

No	$n_{tree}$	$m_{try}$	Rating for performance indices						Total rate	
			Train			Test				
			Rating for $R^2$	Rating for RMSE	Rating for VAF	Rating for $R^2$	Rating for RMSE	Rating for VAF		
1	200	4	8	3	4	4	4	7	8	34
2	150	4	1	8	2	4	11	8	8	34
3	100	4	3	12	4	1	1	2	2	23
4	50	4	3	3	4	1	7	2	2	20
5	200	6	5	3	1	1	9	8	8	27
6	150	6	10	10	11	11	3	1	1	46
7	100	6	7	6	9	8	1	7	7	38
8	50	6	8	1	4	4	4	5	5	26
<b>9</b>	<b>200</b>	<b>8</b>	<b>12</b>	<b>11</b>	<b>12</b>	<b>12</b>	<b>10</b>	<b>12</b>	<b>12</b>	<b>69</b>
10	150	8	10	8	2	4	6	2	2	32
11	100	8	5	6	9	10	12	8	8	50
12	50	8	1	1	8	8	4	5	5	27

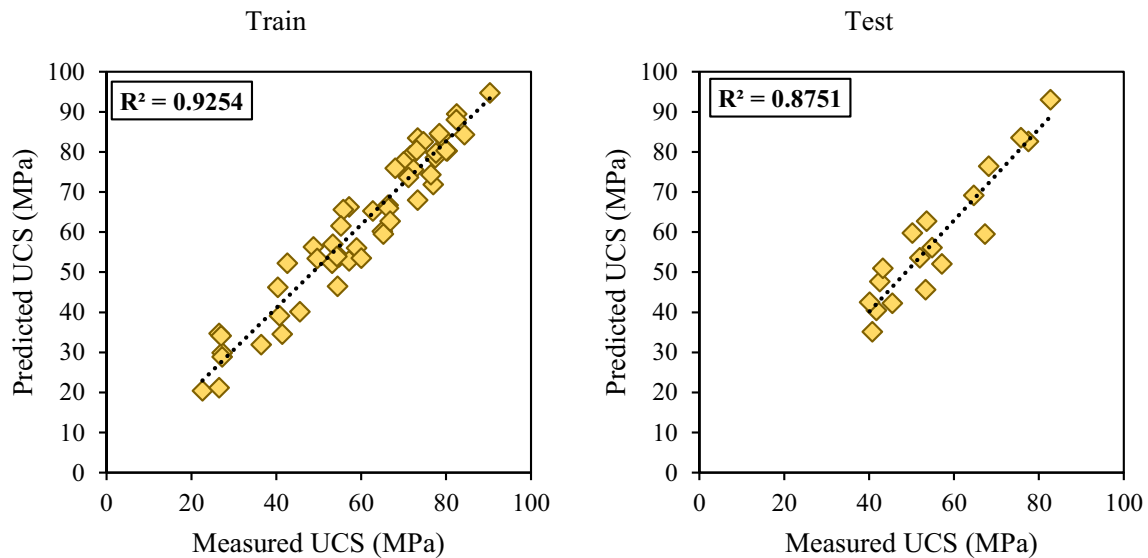


Fig. 12 Measured UCS values compared to predicted one by RF model

### 6.3 Developing ANN model

The UCS values were predicted using three different ANNs: MLP, GFF, and BR. The Levenberg–Markqvist (LM) algorithm was used to overcome the problems corresponding with issues of a complex nature in the system as a learning function and also for training the ANN. In general, the number of the hidden layer(s), the number of neurons in the hidden layer(s), the types of transfer (activation) functions, and the learning algorithms are some of the hyperparameters that manage ANNs efficiency and capabilities. Hence, the accuracy and result of an ANN heavily depend on the mentioned parameters. These parameters were adjusted with various values to find the most appropriate network structure with the highest potential performance. This approach was carried out through trial and error and does not adhere to rules. An extensive summary of the characteristics of the established networks to estimate UCS values is given in Table 5. The transfer functions “purelin”, “logsig”, “tansig”, and “radbas” were examined. The total number of hidden nodes was also selected to be between 3 and 24. As a result, fifteen various structures were constructed. The results of the MLP models with different properties are presented in Table 5. Based on the justification provided for the FRM technique, Eq. (38) was used to score each  $R^2$ , RMSE, and VAF of the training and testing phases. The results revealed that model no. 11, shown in bold, with a structure of 5-11-9-1, a transfer function of “tansig-tansig-logsig”, and a total rate of 88 of 90, was the top-ranked MLP model. As shown in Table 5, the MLP model’s performance level to predict UCS values was shown by  $R^2$  values of 0.904 and 0.859 for the training and testing stages, respectively.

The predicted and measured UCS values are compared in Fig. 13.

The UCS values were also predicted using the GFF neural network approach. The GFF neural networks may solve problems with several complicated correlations between certain issue factors. After normalizing the dataset and dividing it into training and testing datasets, 15 diverse GFF neural network models were created, each with a different learning method, number of hidden nodes, and transfer functions. The topology of the GFF neural network was implemented by using trial and error technique.  $R^2$ , RMSE, and VAF analysis were used to evaluate the model’s accuracy (Table 6). As found in Table 6, the GFF neural network model no. 13 with the architecture 5-13-9-1, shown in bold, was the best model. Notably, the best model’s optimum topology produced the best  $R^2$  (train 0.915, test 0.903), VAF (train 90.988, test 85.268), and RMSE (train 4.655, test 2.624) results. As a result, this model received the highest rating of 90 out of 90. The comparison between measured and predicted UCS values using GFF neural network No. 13 is shown in Fig. 14.

The BR neural network predictive model was also used to estimate the UCS values in this step. The number of hidden neurons in the BR neural network model causes the system complexity. Therefore, the BR neural network modelling is regulated by using the number of hidden nodes as a stopping condition. The number of hidden nodes was changed to fall within the range of 1 to 15 to prevent overfitting and learning problems. They created the 15 BR neural network models. Table 7 summarizes the outcomes of BR neural network modelling for forecasting the UCS values. The best BR neural network model architecture was chosen using the FRM method. With a cumulative rating of

**Table 5** Obtained performance indices and their rates for MLP models

Model	No	Network architecture	Transfer function	Performance indices					
				Train			Test		
				$R^2$	RMSE	VAF	$R^2$	RMSE	VAF
MLP	1	5-3-1	Tansig-tansig	0.897	5.943	85.709	0.806	4.539	84.949
	2	5-5-1	Logsig-tansig	0.877	4.943	80.909	0.720	3.339	77.049
	3	5-7-1	Purelin-tansig	0.891	5.043	88.809	0.780	4.139	81.949
	4	5-9-1	Tansig-purelin	0.851	5.143	81.409	0.846	3.739	85.486
	5	5-5-7-1	Tansig-tansig-tansig	0.841	6.043	81.609	0.820	3.539	80.549
	6	5-5-9-1	Radbas-logsig-purelin	0.837	5.243	88.809	0.820	5.939	85.249
	7	5-7-5-1	Tansig-purelin-tansig	0.851	4.947	82.909	0.766	3.539	82.449
	8	5-7-9-1	Tansig-logsig-radbas	0.877	5.243	89.009	0.780	3.539	81.949
	9	5-9-5-1	Purelin-tansig-tansig	0.891	5.143	88.509	0.856	2.639	83.649
	10	5-9-9-1	Logsig-tansig-purelin	0.901	5.043	80.909	0.780	2.902	82.349
	<b>11</b>	<b>5-11-9-1</b>	<b>Tansig-tansig-logsig</b>	<b>0.904</b>	<b>4.943</b>	<b>90.009</b>	<b>0.860</b>	<b>2.539</b>	<b>85.749</b>
	12	5-13-5-1	Logsig-tansig-tansig	0.807	5.443	82.709	0.846	2.993	76.249
	13	5-13-9-1	Purelin-radbas-tansig	0.824	5.043	89.209	0.860	3.239	83.949
	14	5-15-7-1	Tansig-tansig-purelin	0.847	6.943	87.609	0.806	2.739	84.749
	15	5-15-9-1	Logsig-tansig-radbas	0.877	5.001	90.008	0.780	2.939	81.149

No	Network architecture	Transfer function	Rating for performance indices						Total rate
			Train			Test			
			Rating for $R^2$	Rating for RMSE	Rating for VAF	Rating for $R^2$	Rating for RMSE	Rating for VAF	
1	5-3-1	Tansig-tansig	13	3	7	7	2	12	44
2	5-5-1	Logsig-tansig	8	14	1	1	8	2	34
3	5-7-1	Purelin-tansig	12	9	10	3	3	5	42
4	5-9-1	Tansig-purelin	6	7	3	11	4	14	45
5	5-5-7-1	Tansig-tansig-tansig	4	2	4	9	5	3	27
6	5-5-9-1	Radbas-logsig-purelin	3	5	10	9	1	13	41
7	5-7-5-1	Tansig-purelin-tansig	6	13	6	2	5	8	40
8	5-7-9-1	Tansig-logsig-radbas	8	5	12	3	7	6	41
9	5-9-5-1	Purelin-tansig-tansig	11	7	9	13	14	9	63
10	5-9-9-1	Logsig-tansig-purelin	14	9	1	3	12	7	46
<b>11</b>	<b>5-11-9-1</b>	<b>Tansig-tansig-logsig</b>	<b>15</b>	<b>14</b>	<b>15</b>	<b>14</b>	<b>15</b>	<b>15</b>	<b>88</b>
12	5-13-5-1	Logsig-tansig-tansig	1	4	5	11	10	1	32
13	5-13-9-1	Purelin-radbas-tansig	2	9	13	14	9	10	57
14	5-15-7-1	Tansig-tansig-purelin	5	1	8	7	13	11	45
15	5-15-9-1	Logsig-tansig-radbas	8	12	14	3	11	4	52

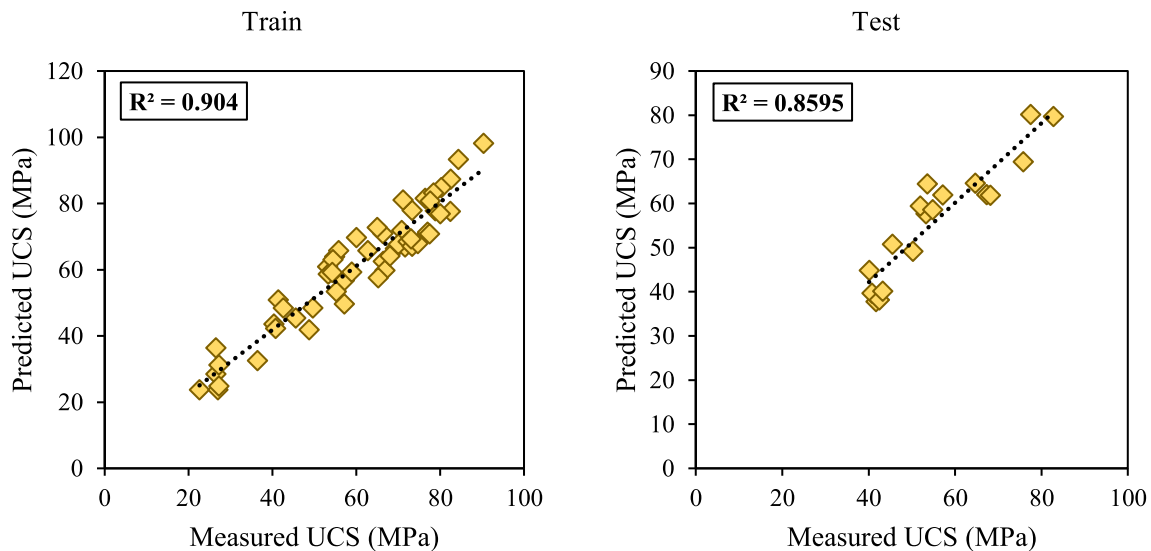


**Fig. 13** Measured UCS compared to predicted one by MLP model

87 out of 95, the BR neural network model number 8, shown in bold, is the one that predicts UCS values with the highest degree of accuracy. The ideal BR neural network model has a 5-8-1 design. It should be noted that these models consider colours that are more vibrant than those in previous BR neural network models. Figure 15 compares ' actual and predicted of UCS values using the best BR neural network model.

#### 6.4 Ensemble model based on WAE-JS hybrid algorithm

The WAE model is established on the concept that more competent base models should have a higher effect on the result. This is performed by providing weight to the result of several models. These weights may be found in several ways. The adoption of metaheuristic optimization algorithms is one of these ideas. In this study, the JS optimization algorithm was used to find the optimal weight of base models, i.e. CART, RF, MLP, GFF, and BR. Like other evolutionary computation techniques, the JS algorithm starts with initially generated solutions. The JS algorithm followed the four main steps to determine the base models' weight.

- (1) The chaotic map procedure was used to create the initial population of the artificial jellyfishes,  $X_i(i = 1, 2, \dots, n)$ :
- (2) The jellyfish represented a model in the search space. The maximum number of iterations in this study and the size of the jellyfish population were set as 1000 and 85, respectively.
- (3) Beta and gamma had respective values of 5 and 0.19 based on trial and error.

- (4) Finding the  $X_*$ :

In this study, the RMSE values are employed to define fitness function as follows (Eq. 16):

$$F_f = \sqrt{\left(\frac{\sum_{i=1}^n (X_i^O - X_i^E)^2}{n_s}\right)} \quad (16)$$

In which,  $X_i^O$ ,  $X_i^E$ ,  $n_s$  are the observed UCS, estimated UCS, and number of data, respectively. An artificial jellyfish with the lowest fitness function was given to the  $X_*$  by the algorithm.

- (3) Up until the maximum number of iterations:
- (4) Determine the time control function,  $c(t)$ , using Eq. (9).
- (5) Run a global or local search for artificial jellyfish.
- (6) Inspect the generated values and replace them with a new one if they fall outside the specified ranges.
- (7) Consider the new value, and if its fitness function value was the lowest, add it to  $X_*$ .
- (8) Output the final weights

Herein, weights to assemble base models in the WAE model are determined using the JS algorithm. Figure 16 shows the WAE model that has been proposed.  $W_i$  is a weight that can be applied to the result of the  $i$ th model in Fig. 16. Therefore, to maintain the following relation,  $\sum_{i=1}^n W_i = 1$ , a value should be randomly chosen between [0, 1]. In this case, RMSE opted as the cost function (minimization).

A comparison of statistical criteria revealed that the CART model is the superior model for predicting UCS values with the best performance and accuracy (Table 8).



**Table 6** Obtained performance indices and their rates for GFF models

Model	No	Network architecture	Performance indices					
			Train			Test		
			$R^2$	RMSE	VAF	$R^2$	RMSE	VAF
GFF	1	5-3-1	0.875	6.655	88.088	0.853	3.624	75.668
	2	5-5-1	0.895	5.255	86.488	0.863	2.994	83.668
	3	5-7-1	0.815	7.555	84.088	0.883	3.674	83.968
	4	5-9-1	0.845	5.355	90.588	0.833	3.332	84.268
	5	5-5-7-1	0.885	4.755	89.788	0.813	2.924	84.368
	6	5-5-9-1	0.875	5.655	89.988	0.873	3.424	81.568
	7	5-7-5-1	0.845	8.026	80.788	0.893	2.824	78.568
	8	5-7-9-1	0.855	5.055	85.888	0.853	2.824	83.868
	9	5-9-5-1	0.904	6.146	90.788	0.883	2.824	81.568
	10	5-9-9-1	0.901	7.013	75.888	0.902	3.424	80.468
	11	5-11-9-1	0.865	5.155	84.688	0.843	3.324	77.768
	12	5-13-5-1	0.855	4.850	88.588	0.833	3.224	80.068
	<b>13</b>	<b>5-13-9-1</b>	<b>0.915</b>	<b>4.655</b>	<b>90.988</b>	<b>0.903</b>	<b>2.624</b>	<b>85.268</b>
	14	5-15-7-1	0.905	4.955	84.388	0.893	2.924	79.468
	15	5-15-9-1	0.845	5.755	81.188	0.873	3.124	82.168

No	Network architecture	Rating for performance indices						Total rate
		Train			Test			
		Rating for $R^2$	Rating for RMSE	Rating for VAF	Rating for $R^2$	Rating for RMSE	Rating for VAF	
1	5-3-1-	8	4	9	5	2	1	29
2	5-5-1-	11	9	8	7	9	10	54
3	5-7-1-	1	2	4	10	1	12	30
4	5-9-1-	2	8	13	2	5	13	43
5	5-5-7-1	10	14	11	1	11	14	61
6	5-5-9-1	8	7	12	8	3	7	45
7	5-7-5-1	2	1	2	12	12	3	32
8	5-7-9-1	5	11	7	5	12	11	51
<b>9</b>	<b>5-9-5-1</b>	<b>13</b>	<b>5</b>	<b>14</b>	<b>10</b>	<b>12</b>	<b>7</b>	<b>61</b>
10	5-9-9-1	12	3	1	14	3	6	39
11	5-11-9-1	7	10	6	4	6	2	35
12	5-13-5-1	5	13	10	2	7	5	42
<b>13</b>	<b>5-13-9-1</b>	<b>15</b>	<b>15</b>	<b>15</b>	<b>15</b>	<b>15</b>	<b>15</b>	<b>90</b>
14	5-15-7-1	14	12	5	12	10	4	57
15	5-15-9-1	2	6	3	8	8	9	36

Therefore, the models were ranked based on their accuracy: CART > GFF > RF > BR > MLP.

In the next step, the final weight of the base model was found using the JS algorithm, as displayed in Fig. 16. Figure 16 shows the convergence diagram of the RMSE to minimal values. Based on the results, base model weights are determined (Fig. 17). The highest and lowest weights are assigned to the CART and MLP models, respectively.

In this step, the ensemble model based on WAE was developed using weighted base models. For this, after developing, evaluating, and comparing the required models, the developed models were subsequently weighted by using the JS algorithm and the final predicted values were obtained using Eq. (17):

$$y_f = \sum_{i=1}^n (w_i \times y_i^{\text{base}}) \tag{17}$$

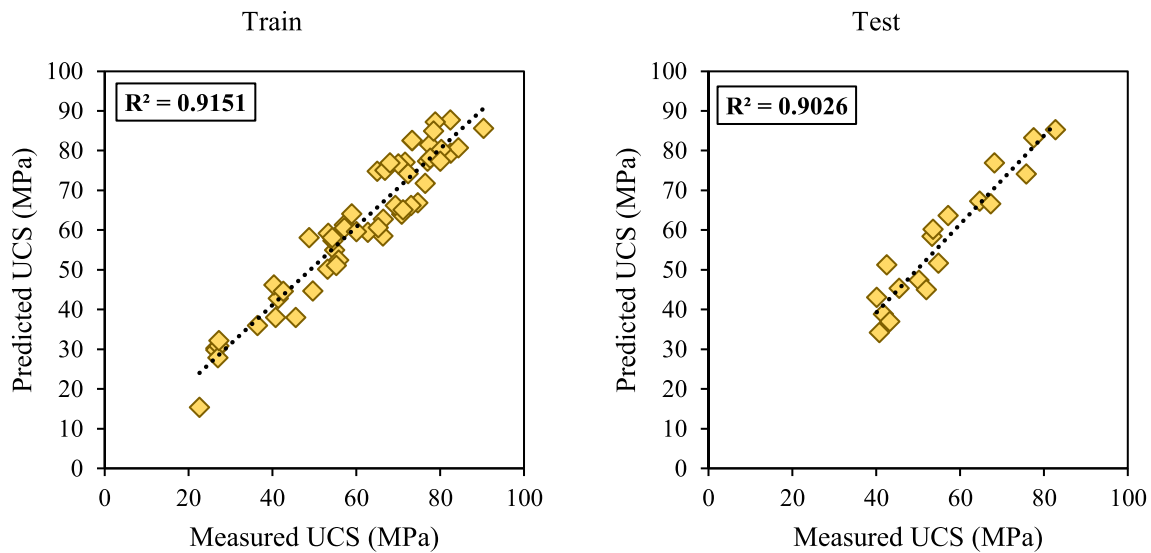


Fig. 14 Measured UCS compared to predicted one by GFF model

where  $y_f$  is the final output from ensemble model,  $w_i$  denotes the weight of each model, and  $y_i^{base}$  indicates the output from each base model (CART, RF, MLP, GFF, and BR).

### 6.5 Evaluation of the predictive models

As mentioned before, the developed models were evaluated utilizing statistical indicators of  $R^2$ , RMSE, and VAF, which were used for measuring the performance of the predictive models. The best model had values close to 1, 0, and 100 for  $R^2$ , RMSE, and VAF, respectively. Therefore, the values of the performance indices were calculated for both training and testing datasets (Fig. 18). As seen, the accuracy and performance level of the WAE model were better than CART, RF, MLP, GFF, and BR. In addition, Fig. 19 demonstrates a comparison between measured and estimated UCS values for the developed model by training and testing datasets. Therefore, the ensemble models presented the most reliable results among each constructed best base model in predicting UCS values in the fully grouted rock bolting system.

Table 9 presents the performance of various ML models for predicting the grout’s UCS values in the fully grouted rock bolting system. The CART, RF, GFF, and BR models showed strong performances with high  $R^2$  values on both the training and testing datasets. The RMSE values are relatively low, indicating good predictive accuracy. However, a decrease in RMSE on the testing datasets was seen in all models. Also, the VAF values are relatively high, indicating a good level of VAF.

Moreover, the WAE-JS model was the clear top performer, exhibiting the highest  $R^2$  values, the lowest RMSE values, and the highest VAF values on both training and testing datasets. It outperformed the other models and

demonstrated minimal signs of overfitting. They generalized effectively to the testing data. Indeed, the WAE-JS model is the standout choice for predicting grout’s UCS values in fully grouted rock bolting systems due to its superior performance across all evaluation metrics.

### 6.6 Sensitivity analyses

To determine the effectiveness of parameters and suggest the most effective parameters on variation UCS values, a sensitivity analysis was carried out for all the input parameters using the cosine amplitude (CA) method. In the CA technique, all data pairs are arranged into a data array (Eq. 18):

$$X = \{x_1, x_2, x_3, \dots, x_i, \dots, x_n\} \tag{18}$$

In which,  $x_i$  stands a vector with the length of  $m$  as Eq. (19):

$$x = \{x_{i1}, x_{i2}, x_{i3}, \dots, x_{ii}, \dots, x_{im}\} \tag{19}$$

Therefore, the sensitivity of each input can be calculated as following formula that establishes the relationships between  $x_i$  and  $x_j$ :

$$r_{ij} = \frac{\sum_{k=1}^m (x_{ik} \times x_{jk})}{\sqrt{(\sum_{k=1}^m x_{ik}^2)} \times \sqrt{(\sum_{k=1}^m x_{jk}^2)}} \tag{20}$$

where  $x_{ik}$  and  $x_{jk}$  are the input and output parameters,  $m$  denotes the number of datasets.

The sensitivity analysis results revealed that W/G had the most impact on the grout’s UCS values among all the inputs (Fig. 20). Based on the calculated effectiveness value ( $r_{ij}$ ), input parameters can be sorted in descending order: CT (0.871), GS (0.834), GF (0.592), and GBU (0.405).

**Table 7** Obtained performance indices and their rates for BR models

Model	No	Network architecture	Performance indices					
			Train			Test		
			$R^2$	RMSE	VAF	$R^2$	RMSE	VAF
BR	1	5-1-1	0.887	5.108	85.691	0.800	3.356	85.064
	2	5-2-1	0.887	5.608	87.691	0.850	3.156	83.964
	3	5-3-1	0.877	5.808	88.591	0.860	4.256	81.364
	4	5-4-1	0.900	5.508	85.891	0.830	4.256	81.664
	5	5-5-1	0.893	5.908	86.191	0.830	3.056	84.864
	6	5-6-1	0.887	4.808	88.891	0.820	3.456	81.464
	7	5-7-1	0.857	5.808	88.391	0.860	4.156	82.464
	<b>8</b>	<b>5-8-1</b>	<b>0.907</b>	<b>5.008</b>	<b>90.191</b>	<b>0.904</b>	<b>2.656</b>	<b>85.664</b>
	9	5-9-1	0.903	6.108	89.691	0.860	3.156	84.864
	10	5-10-1	0.837	5.908	89.791	0.820	3.656	82.964
	11	5-11-1	0.905	6.008	88.591	0.865	3.456	82.164
	12	5-12-1	0.857	5.208	86.391	0.850	4.156	85.764
	13	5-13-1	0.897	6.308	90.083	0.832	3.556	81.164
	14	5-14-1	0.847	6.008	90.491	0.870	3.656	82.764
	15	5-15-1	0.877	5.508	89.291	0.810	2.956	84.464

No	Network architecture	Rating for performance indices						Total rate
		Train			Test			
		Rating for $R^2$	Rating for RMSE	Rating for VAF	Rating for $R^2$	Rating for RMSE	Rating for VAF	
1	5-1-1	7	13	1	1	10	13	45
2	5-2-1	7	9	5	8	11	9	49
3	5-3-1	5	7	7	12	1	2	34
4	5-4-1	12	10	2	5	1	4	34
5	5-5-1	10	5	3	5	13	12	48
6	5-6-1	7	15	9	3	8	3	45
7	5-7-1	3	7	6	10	3	6	35
<b>8</b>	<b>5-8-1</b>	<b>15</b>	<b>14</b>	<b>14</b>	<b>15</b>	<b>15</b>	<b>14</b>	<b>87</b>
9	5-9-1	13	2	11	10	11	11	58
10	5-10-1	1	5	12	3	5	8	34
11	5-11-1	14	3	7	13	8	5	50
12	5-12-1	3	12	4	8	3	15	45
13	5-13-1	11	1	13	7	7	1	40
14	5-14-1	2	3	15	14	5	7	46
15	5-15-1	5	10	10	2	14	10	51

## 7 Conclusions

Mechanical parameters of grouts such as UCS play critical roles in applying ground-controlling methods such as fully grouted rock bolting systems in civil, mining, and geotechnical projects. This research focused on developing

a model ensemble system to predict grouts’s UCS of strata reinforcements’ system. The main novelty of this study was the integration of a new algorithm of JS with the WAE technique, called WAE-JS, to develop an ensemble model. For this purpose, two commercial grouts in the Australian industry, including Stratabinder HS and BU-100, were

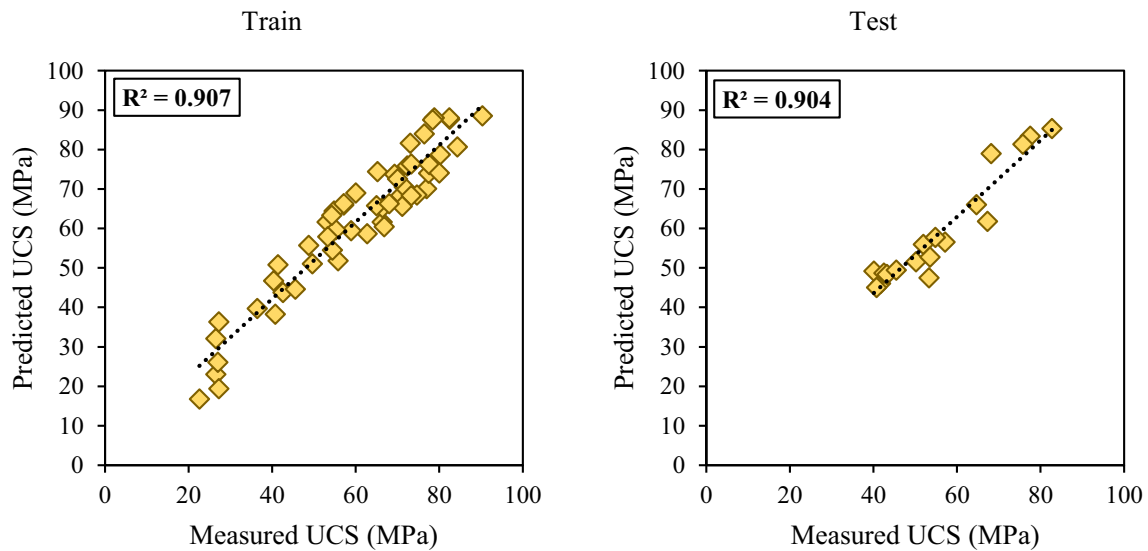
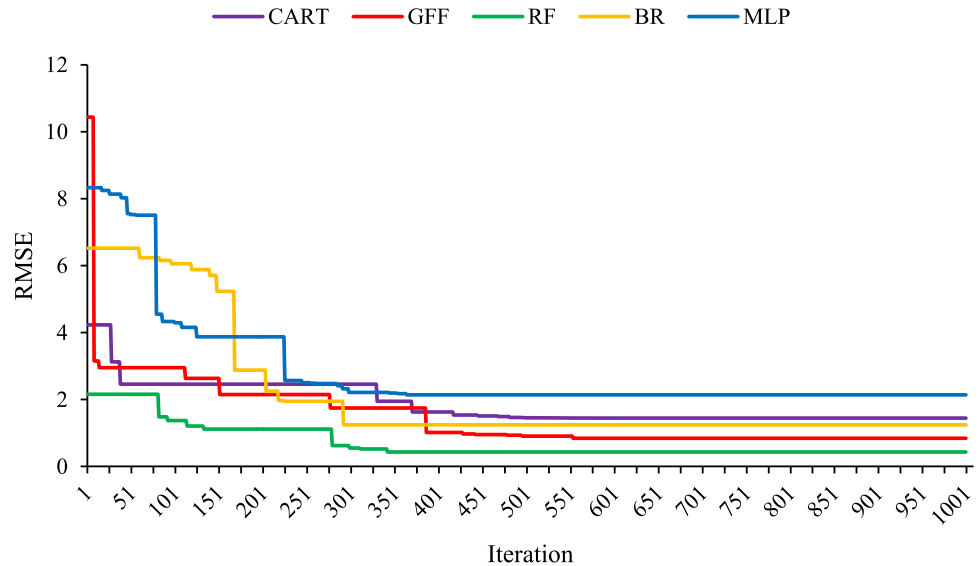


Fig. 15 Measured UCS compared to predicted one by BR neural network model

Fig. 16 Performance of determining the weights of the base models using the JS algorithm



considered for further investigation. Then, comprehensive experimental UCS tests were conducted considering some influential parameters on grout values, such as different curing time ranges, various W/G ratios, and several fly ash contents. After building the dataset, the MLP, BR, GFF, CART, and RF models were used to generate the outputs, while the JS algorithm was employed for weighting obtained outputs. The WAE-JS model consistently outperformed other ML algorithms, as evidenced by high R-squared values, low RMSE values, and exceptional VAF scores for both the training and testing sets. These results proved the reliability and accuracy of this algorithm in

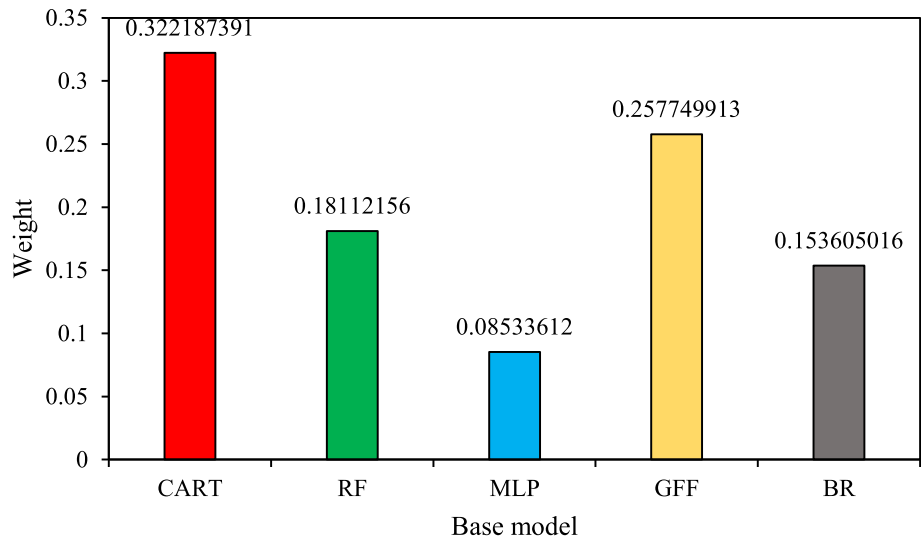
predicting grout UCS values. By replacing traditional, time-consuming, and costly conventional measurement methods with ML techniques, the proposed algorithm can significantly accelerate the UCS prediction process, which is particularly valuable in project planning and decision-making. Also, the WAE-JS model demonstrated remarkable generalization capabilities, as indicated by its minimal overfitting on the testing set. This robustness allows for the application of the model in many practical scenarios. While the presented algorithm exhibited outstanding performance, there are several areas for further investigation and improvement. Enhancing the interpretability of the WAE-

**Table 8** Performance indices for CART, RF, MLP, GFF, and MLP models and their ranks

Model	Rating for performance indices					
	Train			Test		
	$R^2$	RMSE	VAF	$R^2$	RMSE	VAF
CART	0.915	4.835	90.389	0.913	2.424	86.930
RF	0.925	4.852	91.140	0.875	2.772	84.098
MLP	0.904	4.943	90.009	0.860	2.539	85.749
GFF	0.915	4.655	90.988	0.903	2.624	85.268
BR	0.907	5.008	90.191	0.904	2.656	85.664

Model	Rating for performance indices						Total rate	Rank
	Rating for $R^2$	Rating for RMSE	Rating for VAF	Rating for $R^2$	Rating for RMSE	Rating for VAF		
CART	3	4	3	5	5	5	25	1
RF	5	3	5	2	1	1	17	3
MLP	1	2	1	1	4	4	13	5
GFF	3	5	4	3	3	2	20	2
BR	2	1	2	4	2	3	14	4

**Fig. 17** Final weight of the base models



JS model could provide valuable insights into the underlying factors influencing grout’s UCS values. This could aid in better understanding the relationship between input parameters and UCS values. The quality and quantity of data used to train and test the algorithm are critical to its performance. Continual efforts to collect and curate comprehensive datasets are essential. Indeed, the dataset can be

developed by considering the other grout types, additives, and parameters. The development of the WAE-JS ensemble model represented a significant step forward in predicting grout UCS values in the fully grouted rock bolting system, offering exceptional accuracy, efficiency, and generalization capabilities. While the algorithm presented remarkable advantages, addressing challenges related to

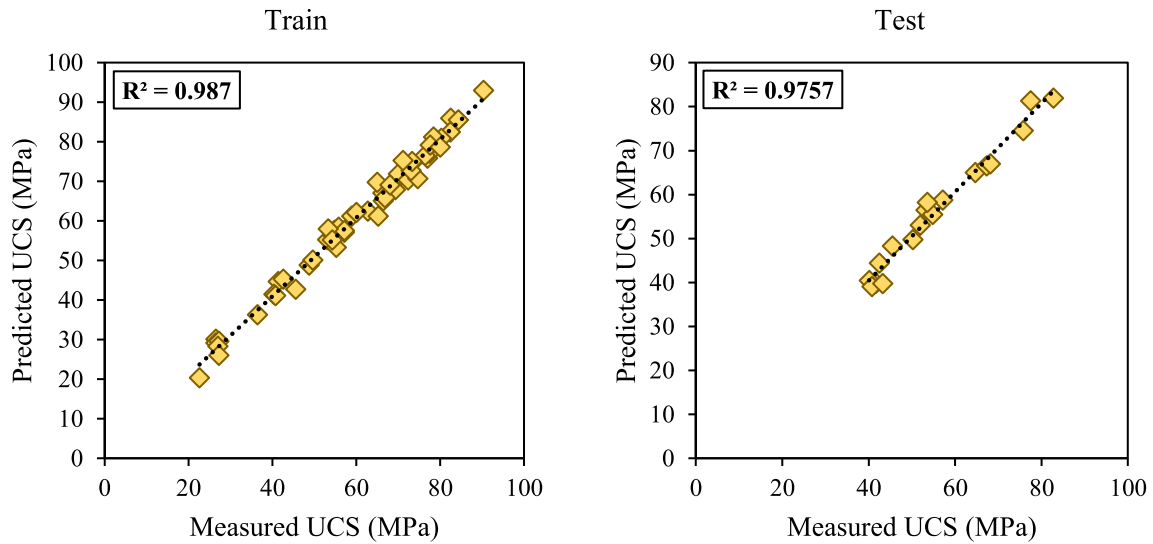


**Fig. 18** Measured UCS compared to predicted one by WAE model

**Fig. 19** Comparison of statistical indices for CART, RF, MLP, GFF, BR, and WAE models

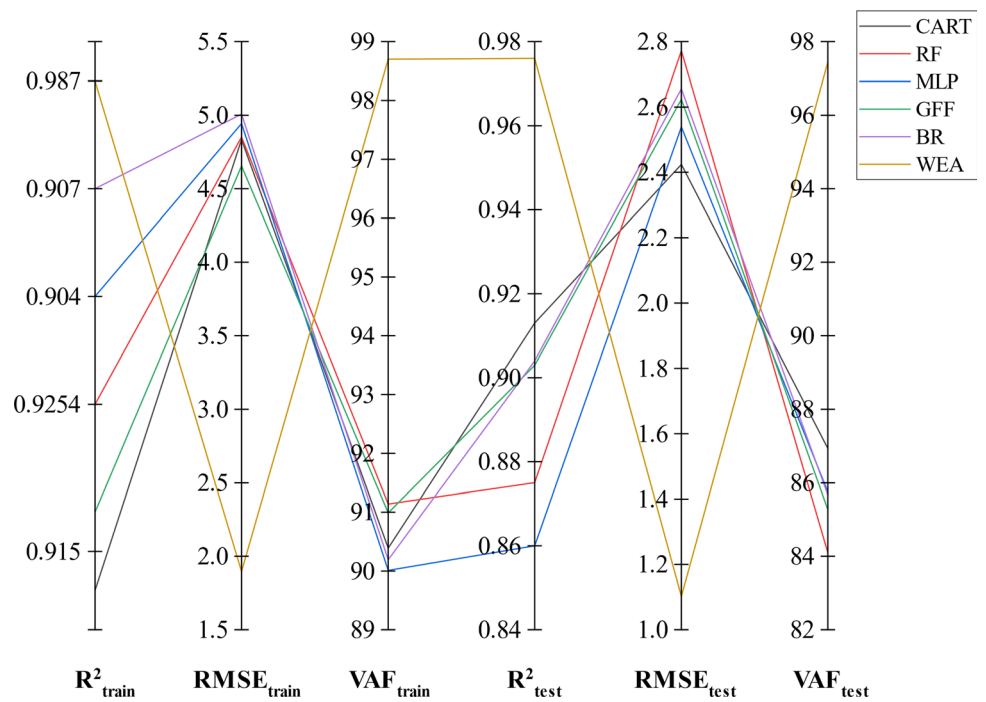


**Table 9** Comparison of developed models based on the evaluation metrics

Model	$R^2$ of train	$R^2$ of test	RMSE of train	RMSE of test	VAF of train	VAF of test
CART	0.915	0.913	4.835	2.424	90.389	86.93
RF	0.925	0.875	4.852	2.772	91.14	84.098
MLP	0.904	0.86	4.943	2.539	90.009	85.749
GFF	0.915	0.903	4.655	2.624	90.988	85.268
BR	0.907	0.904	5.008	2.656	90.191	85.664
WAE-JS	0.987	0.976	1.896	1.102	98.700	97.446

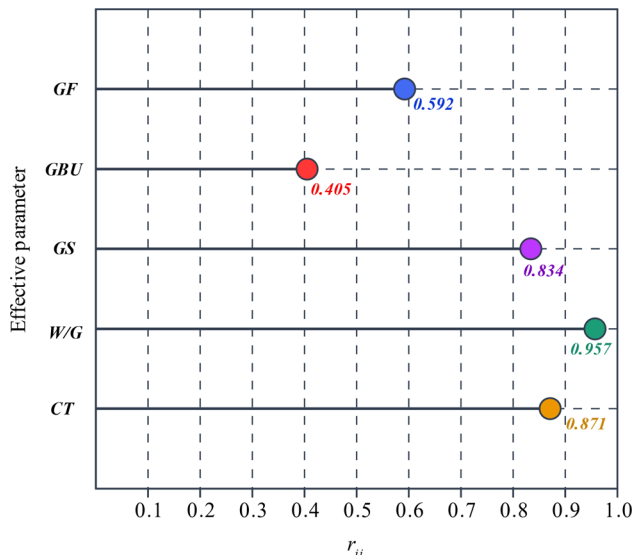


**Fig. 20** Influence degree of effective parameters on UCS

interpretability and real-world validation will further enhance its utility in ground control methods in construction, mining, and geotechnical projects.

**Acknowledgements** Authors would like to acknowledge the in-kind support of Minova and Jenmar and in particular Mr. Robert Hawker and Dr Peter Craig for this research.

**Funding** Open Access funding enabled and organized by CAUL and its Member Institutions.

**Data availability** The data will be made available on your request.

## Declarations

**Conflict of interest** The authors declare that they have no known competing financial interests or personal relationships that could have appeared to influence the work reported in this paper.

**Open Access** This article is licensed under a Creative Commons Attribution 4.0 International License, which permits use, sharing, adaptation, distribution and reproduction in any medium or format, as long as you give appropriate credit to the original author(s) and the source, provide a link to the Creative Commons licence, and indicate if changes were made. The images or other third party material in this article are included in the article's Creative Commons licence, unless indicated otherwise in a credit line to the material. If material is not included in the article's Creative Commons licence and your intended use is not permitted by statutory regulation or exceeds the permitted use, you will need to obtain permission directly from the copyright holder. To view a copy of this licence, visit <http://creativecommons.org/licenses/by/4.0/>.

## References

1. Mirza A, Aziz N, Ye W, Nemicik J (2016) Mechanical properties of grouts at various curing times. In: Paper presented at the proceedings of the 16th coal operators' conference, Wollongong

2. Nourizadeh H, Mirzaghobanali A, McDougall K, Jeewantha LHH, Craig P, Motallebiyan A, Jodeiri Shokri B, Rastegarmanesh A, Aziz N (2023) Characterization of mechanical and bonding properties of anchoring resins under elevated temperature. *Int J Rock Mech Min Sci*. <https://doi.org/10.1016/j.ijrmms.2023.105506>
3. Craig P, and Holden, M (2014) In situ bond strength testing of australian cable bolts. In: Paper presented at the 14th coal operators' conference
4. Jodeiri Shokri B, Entezam S, Nourizadeh H, Motallebiyan A, Mirzaghobanali A, McDougall K, Aziz N, Karunasena K (2023) The effect of changing confinement diameter on axial load transfer mechanisms of fully grouted rock bolts. In: Paper presented at the proceedings of 2023 resource operators conference, University of Wollongong, Wollongong, Australia
5. Blanco Martín L, Tijani M, Hadj-Hassen F, Noiret A (2013) Assessment of the bolt-grout interface behaviour of fully grouted rockbolts from laboratory experiments under axial loads. *Int J Rock Mech Min Sci* 63:50–61. <https://doi.org/10.1016/j.ijrmms.2013.06.007>
6. Aziz N, Majoor D, Mirzaghobanali A (2017) Strength properties of grout for strata reinforcement. *Procedia Eng* 191:1178–1184. <https://doi.org/10.1016/j.proeng.2017.05.293>
7. Craig P, Aziz N, Nemicik J, Moslemi A (2014) Evaluating methods of underground short encapsulation pull testing in australian coal mines. In: Paper presented at the 2014 Coal Operators' Conference, Wollongong
8. Aziz N, Craig P, Mirzaghobanali A, Nemicik J (2016) Factors influencing the quality of encapsulation in rock bolting. *Rock Mech Rock Eng* 49(8):3189–3203. <https://doi.org/10.1007/s00603-016-0973-5>
9. Aziz N, Nemicik J, Mirzaghobanali A, Foldi S, Joyce D, Moslemi A, Ghojavand H, Ma S, Li X, and Rasekh H (2014) Suggested methods for the preparation and testing of various properties of resins and grouts. in: Kininmonth NAAB (Ed.) Proceedings of the 2014 Coal Operators' Conference. University of Wollongong, Wollongong, pp. 163-176
10. Li X, Nemicik J, Mirzaghobanali A, Aziz N, Rasekh H (2015) Analytical model of shear behaviour of a fully grouted cable bolt subjected to shearing. *Int J Rock Mech Min Sci* 80:31–39
11. Hazrati Aghchai M, Maarefvand P, Salari Rad H (2020) Analytically determining bond shear strength of fully grouted rock bolt based on pullout test results. *Periodica Polytechnica Civ Eng*. <https://doi.org/10.3311/PPci.15195>
12. Entezam S, Jodeiri Shokri B, Nourizadeh H, Motallebiyan A, Mirzaghobanali A, McDougall K, Aziz N, Karunasena K (2023) Investigation of the effect of using fly ash in the grout mixture on performing the fully grouted rock bolt systems. In: Paper presented at the proceedings of the 2023 resource operators conference
13. Nourizadeh H, Mirzaghobanali A, Aziz N, McDougall K, Jodeiri Shokri B, Sahebi A, Mottalebiyan A, Entezam S (2023a) Finite element numerical modelling of rock bolt axial behaviour subject to different geotechnical conditions. In: Paper presented at the 2023 resources operators conference (ROC 2023)
14. Gregor P, Mirzaghobanali A, McDougall K, Aziz N, Jodeiri Shokri B (2023) Shear behaviour of fibreglass rock bolts for various pretension loads. *Rock Mech Rock Eng*. <https://doi.org/10.1007/s00603-023-03474-1>
15. Gregor P, Mirzaghobanali A, McDougall K, Aziz N, Jodeiri Shokri B (2024) Investigating shear behaviour of fibreglass rock bolts reinforcing infilled discontinuities for various pretension loads. *Can Geotech J*. <https://doi.org/10.1139/cgj-2022-0619>
16. Ma SA, Naj NJ, Mirzaghobanali A (2017) The effects of installation procedure on bond characteristics of fully grouted

- rock bolts. *Geotechn Test J*. <https://doi.org/10.1520/GTJ20160239>
17. Mirzaghormanali A, Gregor P, Alkandari H, Aziz N, McDougall K (2018) Mechanical behaviours of grout for strata reinforcement. In: Paper presented at the proceedings of the 2018 coal operators' conference, Wollongong
  18. Mirzaghormanali A, Gregor P, Ebrahim Z, Alfahed A, Aziz N, McDougall K (2019) Strength properties of grout for strata reinforcement. In: Paper presented at the proceedings of the 2019 coal operators conference, Wollongong
  19. Entezam S, Jodeiri Shokri B, Doulati Ardejani S, Mirzaghormanali A, McDougall K, Aziz N (2022) Predicting the pyrite oxidation process within coal waste piles using multiple linear regression (mlr) and teaching-learning-based optimization (tlbo) algorithm. In: Paper presented at the 2022 resource operators conference (ROC 2022), Wollongong
  20. Sohrabi P, Jodeiri Shokri B, Dehghani H (2021) Predicting coal price using time series methods and combination of radial basis function (rbf) neural network with time series. *Miner Econ* 36(2):207–216. <https://doi.org/10.1007/s13563-021-00286-z>
  21. Dehghani H, Jodeiri Shokri B, Mohammadzadeh H, Shamsi R, Abbas Salimi N (2021) Predicting and controlling the ground vibration using gene expression programming (gep) and teaching-learning-based optimization (tlbo) algorithms. *Environ Earth Sci*. <https://doi.org/10.1007/s12665-021-10052-7>
  22. Shamsi R, Amini MS, Dehghani H, Bascompta M, Jodeiri Shokri B, Entezam S (2022) Prediction of fly-rock using gene expression programming and teaching-learning-based optimization algorithm. *J Min Environ (JME)* 13(2):391–406. <https://doi.org/10.22044/jme.2022.11825.2171>
  23. Hosseini S, Mousavi A, Monjezi M (2022) Prediction of blast-induced dust emissions in surface mines using integration of dimensional analysis and multivariate regression analysis. *Arab J Geosci*. <https://doi.org/10.1007/s12517-021-09376-2>
  24. Hosseini S, Poormirzaee R, Hajihassani M, Kalatehjari R (2022) An ann-fuzzy cognitive map-based z-number theory to predict flyrock induced by blasting in open-pit mines. *Rock Mech Rock Eng* 55(7):4373–4390. <https://doi.org/10.1007/s00603-022-02866-z>
  25. Jiskani IM, Yasli F, Hosseini S, Rehman AU, Uddin S (2022) Improved z-number based fuzzy fault tree approach to analyze health and safety risks in surface mines. *Resour Policy*. <https://doi.org/10.1016/j.resourpol.2022.102591>
  26. Jodeiri Shokri B, Ramazi H, Doulati Ardejani F, Sadeghiamirshahidi M (2014) Prediction of pyrite oxidation in a coal washing waste pile applying artificial neural networks (anns) and adaptive neuro-fuzzy inference systems (anfis). *Mine Water Environ* 33(2):146–156. <https://doi.org/10.1007/s10230-013-0247-3>
  27. Mostafaei K, Maleki S, Jodeiri Shokri B, Yousefi M (2023) Predicting gold grade by using support vector machine and neural network to generate an evidence layer for 3d prospectivity analysis. *Int J Min Geo-Eng* 57(4):435–444. <https://doi.org/10.22059/ijmge.2023.362951.595087>
  28. Dehghani H, Velicković M, Jodeiri B, Mihajlović I, Nikolić D, Panic M (2022) Determination of ozone concentration using gene expression programming algorithm (gep)- zrenjanin, serbia. *Int J Min Geo-Eng* 56(1):1–9. <https://doi.org/10.22059/ijmge.2021.313278.594874>
  29. Shamsi R, Dehghani H, Jalali M, Jodeiri Shokri B (2021) Ore grade estimation using the imperialist competitive algorithm (ica). *Arab J Geosci* 14(14):1409. <https://doi.org/10.1007/s12517-021-07808-7>
  30. Dehghani H, Jodeiri B, Sadeghi M (2021) Ultimate pit limit determination using flashlight algorithm. *Int J Mini Geo-Eng* 55(1):43–48. <https://doi.org/10.22059/ijmge.2020.296120.594840>
  31. Jodeiri Shokri B, Dehghani H, Shamsi R, Doulati Ardejani F (2020) Prediction of acid mine drainage generation potential of a copper mine tailings using gene expression programming-a case study. *J Min Environ* 11(4):1127–1140. <https://doi.org/10.22044/jme.2020.10031.1938>
  32. Shakeri J, Jodeiri Shokri B, Dehghani H (2020) Prediction of blast-induced ground vibration using gene expression programming (gep), artificial neural networks (anns), and linear multivariate regression (lmr). *Arch Min Sci* 65(2):317–335. <https://doi.org/10.24425/ams.2020.133195>
  33. Doulati Ardejani F, Rooki R, Jodieri Shokri B, Eslam Kish T, Aryafar A, Tourani P (2013) Prediction of rare earth elements in neutral alkaline mine drainage from razi coal mine, golestan province, northeast iran, using general regression neural network. *J Environ Eng* 139(6):896–907. [https://doi.org/10.1061/\(ASCE\)EE.1943-7870.0000689](https://doi.org/10.1061/(ASCE)EE.1943-7870.0000689)
  34. Meulenkamp F, Grima MA (1999) Application of neural networks for the prediction of the unconfined compressive strength (ucs) from equotip hardness. *Int J Rock Mech Min Sci* 36:29–39
  35. Sonmez H, Tuncay E, Gokceoglu C (2004) Models to predict the uniaxial compressive strength and the modulus of elasticity for ankara agglomerate. *Int J Rock Mech Min Sci* 41(5):717–729. <https://doi.org/10.1016/j.ijrmm.2004.01.011>
  36. Tiryaki B (2008) Predicting intact rock strength for mechanical excavation using multivariate statistics, artificial neural networks, and regression trees. *Eng Geol* 99(1–2):51–60. <https://doi.org/10.1016/j.enggeo.2008.02.003>
  37. Jahed Armaghani D, Tonnizam Mohamad E, Hajihassani M, Yagiz S, Motaghedi H (2015) Application of several non-linear prediction tools for estimating uniaxial compressive strength of granitic rocks and comparison of their performances. *Eng Comput* 32(2):189–206. <https://doi.org/10.1007/s00366-015-0410-5>
  38. Jahed Armaghani D, Safari V, Fahimifar A, Mohd Amin MF, Monjezi M, Mohammadi MA (2017) Uniaxial compressive strength prediction through a new technique based on gene expression programming. *Neural Comput Appl* 30(11):3523–3532. <https://doi.org/10.1007/s00521-017-2939-2>
  39. Moussas VC, Diamantis K (2021) Predicting uniaxial compressive strength of serpentinites through physical, dynamic and mechanical properties using neural networks. *J Rock Mech Geotechn Eng* 13(1):167–175. <https://doi.org/10.1016/j.jrmge.2020.10.001>
  40. Diamantis KMV (2021) Estimating uniaxial compressive strength of peridotites from simple tests using neural networks. *Arab J Geosci* 14:2690
  41. Cao J, Gao J, Nikafshan Rad H, Mohammed AS, Hasanipanah M, Zhou J (2021) A novel systematic and evolved approach based on xgboost-firefly algorithm to predict young's modulus and unconfined compressive strength of rock. *Eng Comput* 38(S5):3829–3845. <https://doi.org/10.1007/s00366-020-01241-2>
  42. Gowida A, Elkatatny S, Gamal H (2021) Unconfined compressive strength (ucs) prediction in real-time while drilling using artificial intelligence tools. *Neural Comput Appl* 33(13):8043–8054. <https://doi.org/10.1007/s00521-020-05546-7>
  43. Azimian A, Ajalloeian R, Fatehi L (2013) An empirical correlation of uniaxial compressive strength with p-wave velocity and point load strength index on marly rocks using statistical method. *Geotech Geol Eng* 32(1):205–214. <https://doi.org/10.1007/s10706-013-9703-x>
  44. Mohamad ET, Jahed Armaghani D, Momeni E, Abad ANK (2014) Prediction of the unconfined compressive strength of soft rocks: a pso-based ann approach. *Bull Eng Geol Env* 74(3):745–757. <https://doi.org/10.1007/s10064-014-0638-0>
  45. Najibi AR, Ghafoori M, Lashkaripour GR, Asef MR (2015) Empirical relations between strength and static and dynamic elastic properties of asmari and sarvak limestones, two main oil



- reservoirs in iran. *J Petrol Sci Eng* 126:78–82. <https://doi.org/10.1016/j.petrol.2014.12.010>
46. Tandon RS, Gupta V (2014) Estimation of strength characteristics of different himalayan rocks from schmidt hammer rebound, point load index, and compressional wave velocity. *Bull Eng Geol Env* 74(2):521–533. <https://doi.org/10.1007/s10064-014-0629-1>
  47. Ng I-T, Yuen K-V, Lau C-H (2015) Predictive model for uniaxial compressive strength for grade iii granitic rocks from macao. *Eng Geol* 199:28–37. <https://doi.org/10.1016/j.enggeo.2015.10.008>
  48. Fereidooni D (2016) Determination of the geotechnical characteristics of hornfelsic rocks with a particular emphasis on the correlation between physical and mechanical properties. *Rock Mech Rock Eng* 49(7):2595–2608. <https://doi.org/10.1007/s00603-016-0930-3>
  49. Jalali SH, Heidari M, Mohseni H (2017) Comparison of models for estimating uniaxial compressive strength of some sedimentary rocks from qom formation. *Environ Earth Sci*. <https://doi.org/10.1007/s12665-017-7090-y>
  50. Sharma LK, Vishal V, Singh TN (2017) Developing novel models using neural networks and fuzzy systems for the prediction of strength of rocks from key geomechanical properties. *Measurement* 102:158–169. <https://doi.org/10.1016/j.measurement.2017.01.043>
  51. Heidari M, Mohseni H, Jalali SH (2017) Prediction of uniaxial compressive strength of some sedimentary rocks by fuzzy and regression models. *Geotech Geol Eng* 36(1):401–412. <https://doi.org/10.1007/s10706-017-0334-5>
  52. Aboutaleb S, Behnia M, Bagherpour R, Bluekian B (2017) Using non-destructive tests for estimating uniaxial compressive strength and static young's modulus of carbonate rocks via some modeling techniques. *Bull Eng Geol Env* 77(4):1717–1728. <https://doi.org/10.1007/s10064-017-1043-2>
  53. Ghasemi E, Kalhori H, Bagherpour R, Yagiz S (2016) Model tree approach for predicting uniaxial compressive strength and young's modulus of carbonate rocks. *Bull Eng Geol Env* 77(1):331–343. <https://doi.org/10.1007/s10064-016-0931-1>
  54. Saedi B, Mohammadi SD, Shahbazi H (2019) Application of fuzzy inference system to predict uniaxial compressive strength and elastic modulus of migmatites. *Environ Earth Sci*. <https://doi.org/10.1007/s12665-019-8219-y>
  55. Aliyu MM, Shang J, Murphy W, Lawrence JA, Collier R, Kong F, Zhao Z (2019) Assessing the uniaxial compressive strength of extremely hard cryptocrystalline flint. *Int J Rock Mech Min Sci* 113:310–321. <https://doi.org/10.1016/j.ijrmms.2018.12.002>
  56. Teymen A, Mengüç EC (2020) Comparative evaluation of different statistical tools for the prediction of uniaxial compressive strength of rocks. *Int J Min Sci Technol* 30(6):785–797. <https://doi.org/10.1016/j.ijmst.2020.06.008>
  57. Mahmoodzadeh A, Mohammadi M, Hashim Ibrahim H, Nariman Abdulhamid S, Ghafoor Salim S, Farid Hama Ali H, Kamal Majeed M (2021) Artificial intelligence forecasting models of uniaxial compressive strength. *Transp Geotechn.* <https://doi.org/10.1016/j.trgeo.2020.100499>
  58. Xu BTY, Sun W, Ma T, Liu H, Wang D (2023) Study on the prediction of the uniaxial compressive strength of rock based on the ssa-xgboost model. *Sustainability* 15(6):5201
  59. Liu Z, Li D, Liu Y, Yang B, Zhang Z-X (2023) Prediction of uniaxial compressive strength of rock based on lithology using stacking models. *Rock Mech Bull.* <https://doi.org/10.1016/j.rockmb.2023.100081>
  60. ASTM (2006) Standard test methods for compressive strength of chemical-resistant mortars, grouts, monolithic surfacings, and polymer concretes.1–4
  61. Li B-F, Olshen R, Stone C (1984) Biometrics 40:358–361 (1984) Classification and regression trees (cart). *Biometrics* 40:358–361. <https://doi.org/10.1201/9781315139470>
  62. Coimbra R, Rodriguez-Galiano V, Olóriz F, Chica-Olmo M (2014) Regression trees for modeling geochemical data—an application to late jurassic carbonates (ammonitico rosso). *Comput Geosci* 73:198–207. <https://doi.org/10.1016/j.cageo.2014.09.007>
  63. Breiman L (2001) Random forests. *Mach Learn* 45:5–32. <https://doi.org/10.1023/A:1010933404324>
  64. Hosseini S, Pourmirzaee R, Armaghani DJ, Sabri Sabri MM (2023) Prediction of ground vibration due to mine blasting in a surface lead-zinc mine using machine learning ensemble techniques. *Sci Rep* 13(1):6591. <https://doi.org/10.1038/s41598-023-33796-7>
  65. Zhao J, Hosseini S, Chen Q, Jahed Armaghani D (2023) Super learner ensemble model: a novel approach for predicting monthly copper price in future. *Resour Policy.* <https://doi.org/10.1016/j.resourpol.2023.103903>
  66. Bakhtavar E, Hosseini S, Hewage K, Sadiq R (2021) Air pollution risk assessment using a hybrid fuzzy intelligent probability-based approach: Mine blasting dust impacts. *Nat Resour Res* 30(3):2607–2627. <https://doi.org/10.1007/s11053-020-09810-4>
  67. Wang X, Hosseini S, Jahed Armaghani D, Tonnizam Mohamad E (2023) Data-driven optimized artificial neural network technique for prediction of flyrock induced by boulder blasting. *Mathematics.* <https://doi.org/10.3390/math11102358>
  68. Mackey D (1992) Bayesian methods for adaptive models. *Calif Inst Technol*
  69. Bui DTPB, Lofman O et al (2012) Landslide susceptibility assessment in the hoa binh province of vietnam: a comparison of the levenberg–marquardt and bayesian regularized neural networks. *Geomorphology* 171:12–29
  70. Hosseini S, Pourmirzaee R (2024) Green policy for managing blasting induced dust dispersion in open-pit mines using probability-based deep learning algorithm. *Expert Syst Appl.* <https://doi.org/10.1016/j.eswa.2023.122469>
  71. Wang Q, Qi J, Hosseini S, Rasekh H, Huang J (2023) Ica-lightgbm algorithm for predicting compressive strength of geo-polymer concrete. *Buildings.* <https://doi.org/10.3390/buildings13092278>
  72. Chou JSTD (2021) A novel metaheuristic optimizer inspired by behavior of jellyfish in ocean. *Appl Math Comput* 389:125535
  73. JH H, (1992) Genetic algorithm. *Sci Am* 267(1):66–73
  74. Rashedi E, Nezamabadi-pour H, Saryazdi S (2009) Gsa: a gravitational search algorithm. *Inf Sci* 179(13):2232–2248. <https://doi.org/10.1016/j.ins.2009.03.004>
  75. Kennedy JER (1995) Particle swarm optimization. Paper presented at the In: Proceedings of the international conference on neural networks; institute of electrical and electronics engineers (IEEE)
  76. Abdel-Basset M, Mohamed R, Chakraborty RK, Ryan MJ, El-Fergany A (2021) An improved artificial jellyfish search optimizer for parameter identification of photovoltaic models. *Energies.* <https://doi.org/10.3390/en14071867>
  77. Kave A, Biabani Hamedani M, Kamalinejad M, Joudaki A (2022) Quantum-based jellyfish search optimizer for structural optimization. *Int J Optim Civ Eng* 11(2):329–356
  78. Gouda EA, Kotb MF, El-Fergany AA (2021) Jellyfish search algorithm for extracting unknown parameters of pem fuel cell models: steady-state performance and analysis. *Energy.* <https://doi.org/10.1016/j.energy.2021.119836>
  79. Truong D-N, Chou J-S (2022) Fuzzy adaptive jellyfish search-optimized stacking machine learning for engineering planning and design. *Autom Constr.* <https://doi.org/10.1016/j.autcon.2022.104579>

80. Alam A, Verma P, Tariq M, Sarwar A, Alamri B, Zahra N, Urooj S (2021) Jellyfish search optimization algorithm for mpp tracking of pv system. *Sustainability*. <https://doi.org/10.3390/su132111736>
81. El-Ashmawi WH, Salah A, Bekhit M, Xiao G, Al Ruqeishi K, Fathalla A (2023) An adaptive jellyfish search algorithm for packing items with conflict. *Mathematics*. <https://doi.org/10.3390/math11143219>
82. Ansari S, Ayob A, Hossain Lipu MS, Hussain A, Md Saad MH (2024) Jellyfish optimized recurrent neural network for state of health estimation of lithium-ion batteries. *Expert Syst Appl*. <https://doi.org/10.1016/j.eswa.2023.121904>
83. Kuo RJ, Chiu T-H (2024) Hybrid of jellyfish and particle swarm optimization algorithm-based support vector machine for stock market trend prediction. *Appl Soft Comput*. <https://doi.org/10.1016/j.asoc.2024.111394>
84. Durmus A, Kurban R, Karakose E (2021) A comparison of swarm-based optimization algorithms in linear antenna array synthesis. *J Comput Electron* 20(4):1520–1531. <https://doi.org/10.1007/s10825-021-01711-w>
85. Brotz L, Cheung WWL, Kleisner K, Pakhomov E, Pauly D (2012) Increasing jellyfish populations: trends in large marine ecosystems. *Hydrobiologia* 690(1):3–20. <https://doi.org/10.1007/s10750-012-1039-7>
86. Mariottini GL, Pane L (2010) Mediterranean jellyfish venoms: a review on scyphomedusae. *Mar Drugs* 8(4):1122–1152. <https://doi.org/10.3390/md8041122>
87. Luo KJY, Zhu J (2021) Perturbation observer based fractional-order control for smes systems based on jellyfish search algorithm. *Front Energy Res* 9:781774. <https://doi.org/10.3389/fenrg.2021.781774>
88. Chou JS, Tjandrakusuma S, Liu CY (2022) Jellyfish search-optimized deep learning for compressive strength prediction in images of ready-mixed concrete. *Comput Intell Neurosci* 2022:9541115. <https://doi.org/10.1155/2022/9541115>
89. R P, (2022) Seismic refraction data inversion via jellyfish search algorithm for bedrock characterization in dam sites. *SN Appl Sci* 4:228. <https://doi.org/10.1007/s42452-022-05171-0>
90. Hosseini S MM (2023) Application of artificial intelligence technique and multi objective grasshopper optimization algorithm for mineto-crusher optimization in surface mines. <https://doi.org/10.20944/preprints202308.0892.v1>
91. Zhou J, Su Z, Hosseini S, Tian Q, Lu Y, Luo H, Xu X, Chen C, Huang J (2024) Decision tree models for the estimation of geopolymer concrete compressive strength. *Math Biosci Eng* 21(1):1413–1444. <https://doi.org/10.3934/mbe.2024061>
92. Hosseini S, Javanshir S, Sabeti H, Tahmasebizadeh P (2023) Mathematical-based gene expression programming (gep): a novel model to predict zinc separation from a bench-scale bioleaching process. *J Sustain Metall* 9(4):1601–1619. <https://doi.org/10.1007/s40831-023-00751-9>
93. Lawal AI, Hosseini S, Kim M, Ogunsola NO, Kwon S (2023) Prediction of factor of safety of slopes using stochastically modified ann and classical methods: a rigorous statistical model selection approach. *Nat Hazards* 120(2):2035–2056. <https://doi.org/10.1007/s11069-023-06275-5>
94. Jodeiri Shokri B, Dehghani H, Shamsi R (2020) Predicting silver price by applying a coupled multiple linear regression (mlr) and imperialist competitive algorithm (ica). *Metaheuristic Comput Appl* 1(1):101–114. <https://doi.org/10.12989/mca.2020.1.1.101>
95. Hosseini S, Monjezi M, Bakhtavar E (2022) Minimization of blast-induced dust emission using gene-expression programming and grasshopper optimization algorithm: a smart mining solution based on blasting plan optimization. *Clean Technol Environ Policy* 24:2313–2328. <https://doi.org/10.1007/s10098-022-02327-9>
96. Jodeiri Shokri B, Mirzaghobanali A, Nourizadeh H, McDougall K, Karunasena W, Aziz N, Entezam S, and Entezam A (2024) Axial load transfer mechanism in fully grouted rock bolting system: a systematic review. *Appl Sci* 14(12):5232. <https://doi.org/10.3390/app14125232>
97. Hosseini S, Jodeiri Shokri B, Mirzaghobanali A, Nourizadeh H, Entezam S, Motallebiyan A, Entezam A, McDougall K, Karunasena W, Aziz N (2024) Predicting axial-bearing capacity of fully grouted rock bolting systems by applying an ensemble system. *Soft Comput*. <https://doi.org/10.1007/s00500-024-09828-3>

**Publisher's Note** Springer Nature remains neutral with regard to jurisdictional claims in published maps and institutional affiliations.